Structure, Thermochemical Properties, and Growth Sequence of Aluminum-Doped Silicon Clusters Si n Al m (n = 1−11, m = 1−2) and Their Anions

4 AUTHORS, INCLUDING:

Minh Tho Nguyen
University of Leuven
748 PUBLICATIONS   10,835 CITATIONS

SEE PROFILE

Truong Tai
University of Leuven
65 PUBLICATIONS   506 CITATIONS

SEE PROFILE

Vu Thi Ngan
Quy Nhon University
32 PUBLICATIONS   558 CITATIONS

SEE PROFILE

Structure, Thermochemical Properties, and Growth Sequence of Aluminum-Doped Silicon Clusters Si_nAl_m (n = 1−11, m = 1−2) and Their Anions

Nguyen Minh Tam,[†,‡] Truong Ba Tai,[‡] Vu Thi Ngan,[§] and Minh Tho Nguyen*[,‡]

[†]Institute for Computational Science and Technology at Ho Chi Minh City (ICST), Vietnam
[‡]Department of Chemistry, University of Leuven, B-3001 Leuven, Belgium
[§]Faculty of Chemistry, Quy Nhon University, Quy Nhon City, Vietnam

Ⓢ Supporting Information

ABSTRACT: A systematic examination of the aluminum doped silicon clusters, Si_nAl_m with n = 1−11 and m = 1−2, in both neutral and anionic states, is carried out using quantum chemical calculations. Lowest-energy equilibrium structures of the clusters considered are identified on the basis of G4 energies. High accuracy total atomization energies and thermochemical properties are determined for the first time using the G4 and CCSD(T)/CBS (coupled-cluster theory with complete basis set up to n = 3) methods. In each size, substitution of Si atoms at different positions of a corresponding pure silicon clusters by Al dopants invariably leads to a spectrum of distinct binary structures but having similar shape and comparable energy content. Such an energetic degeneracy persists in the larger cluster sizes, in particular for the anions. The equilibrium growth sequences for Al-doped Si clusters emerge as follows: (i) neutral *singly doped* Si_nAl clusters favor Al atom substitution into a Si position in the structure of the corresponding cation Si_{n+1}^{+}, whereas the anionic Si_nAl^{-} has one Si atom of the isoelectronic neutral Si_{n+1} being substituted by the Al impurity; and (ii) for *doubly doped* $Si_nAl_2^{0/-}$ clusters, the neutrals have the shape of Si_{n+1} counterparts in which one Al atom substitutes a Si atom and the other Al adds on an edge or a face of it, whereas the anions have both Al atoms substitute two Si atoms in the Si_{n+2}^{+} frameworks. The Al dopant also tends to avoid high coordination position.
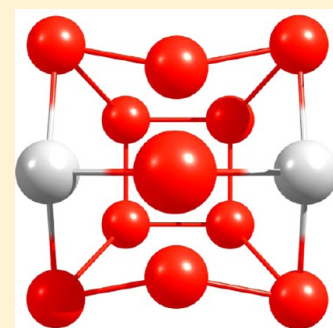
Structure of $Si_{11}Al_2$

1. INTRODUCTION

Clusters of the elements continue to attract much attention, in part due to their large range of unusual physicochemical properties and many promising applications. One of the most interesting characteristics of atomic clusters is that they can be formed by aggregating atoms of either one or several chemical elements. The latter opens a great channel to design new mixed cluster materials whose physicochemical properties can fundamentally differ from those of their parents.

Over the two past decades, a large number of binary clusters containing two different chemical elements were extensively investigated by both experiment and theory. However, most previous studies focused on binary clusters with only one impure atom. Although a number of studies on mixed alloy metallic clusters have been carried out,[1] relatively less is known on impurity-rich binary nonmetal clusters, despite the fact that it is of importance to have a better understanding about mixed materials. From a theoretical viewpoint, one of the main reasons for such a lack of reports is that the search for their global minima is a difficult and tedious task, owing to the huge number of local minima located on their potential energy surfaces. As a consequence, impurity-rich binary clusters present an urgent and necessary target for detailed studies.

Silicon based clusters are of great interest owing to their potential applications in semiconductor and optoelectronic industries.[2−13] The characteristics of electronic structure, spectroscopy, and thermochemical properties of small silicon clusters in various charge states have carefully been studied in the literature. More interestingly, since the first experimental observation for the existence of endohedral transition metal doped silicon clusters was reported,[14] a large number of studies on doped Si clusters were performed with the aim to determine their electronic and magnetic properties and stabilities.[15−47] Recently, we carried out several combined experimental spectrometric and theoretical studies on doped silicon clusters Si_nM with M = Li, Be, B, V, Mn, and Cu.[47−50,50−52] Our extensive findings indicated that, while Li and Cu prefer to be absorbed on the surface of silicon hosts, V-doped clusters Si_nV^+ are built up by substituting one Si-atom of the Si_{n+1}^+ frameworks by one V-dopant. In addition, the endohedrally doped structures with encapsulated impurities were also found at some special sizes. For instance, Be and B were found to be located at the center of Si_8 and Si_{10} hosts.[49,52] Some transition metals are also encapsulated into larger Si_n cages with n = 12, 14, and 16.[52−55]

Among impure silicon materials, the aluminum−silicon mixture gives rise to quite intriguing compounds. Previous studies also

showed considerable significance of aluminum−silicon compounds in nanomaterials fields.[56−58] The Si nanowire interacted by one Al-atom has been found to enhance electrical conductivity as compared to pristine Si-nanowire.[56] Kotlyar et al.[57] found that Al atoms form an ordered array of magic clusters on the surfaces of Si(111). Paulose and co-workers[58] also reported the persistent formation of Al−Si nanowires. In this context, some studies on small binary Al−Si clusters were performed. Sun et al.[59] carried out an experimental study on Si_nB^- and Si_nAl^- anionic clusters (with $n = 1−6$) using a laser ablation technique and time-of-flight mass spectrometry. The geometric structures of these clusters were also investigated theoretically using density functional theory (DFT) method. Subsequently, geometrical features and stabilities of the $Si_nAl^{−/0/+}$ clusters with $n = 2−21$ were examined by Li et al.[60] using full-potential linear-muffin-tin-orbital molecular dynamics (FP-LMTO-MD) method. However, according to our best knowledge, investigations on multiple aluminum doped silicon clusters have not been available yet. In addition, thermochemical properties of the Si_nAl clusters that are fundamental information for subsequent experimental studies, have not been determined in earlier reports.

Motivated by the above reasons, we set out to perform a systematic investigation on a series of small singly and doubly aluminum doped silicon cluster Si_nAl_m with $n = 1−11$ and $m = 1−2$, in both neutral and anionic states. Using the composite G4 energies, we determine the geometries of the lowest-lying equilibrium structures and thereby to probe their growth pattern. Thermochemical properties of the clusters are calculated using both high accuracy G4 and coupled-cluster theory CCSD(T)/CBS approaches that were effectively used in our recent study on boron-doped silicon clusters Si_nB.[50]

2. COMPUTATIONAL METHODS

All electronic structure calculations are carried out using the Gaussian09[61] and Molpro2009[62] program packages. The searches for energy minima are conducted using different approaches. In the first, we use a stochastic genetic algorithm to generate all possible structures.[63] The equilibrium structures that are initially detected using low-level computations are reoptimized using a higher level method. In the second approach, initial structures of clusters Si_nAl are manually constructed by either substituting one Si-atom of the Si_{n+1} frameworks by one Al-atom or adding one Al-atom at various positions on surfaces of the Si_n clusters. Similarly, the initial structures of Si_nAl_2 clusters are generated from known structures of pure silicon clusters and singly aluminum doped silicon clusters Si_nAl. In addition, the local energy minima of Si_nX_m clusters previously reported are also used as referenced structures.

The use of the genetic algorithm is less effective for producing singly doped-clusters having small sizes because most of the relevant structures in silicon clusters are relatively well-known. On the contrary, the multidoped and larger size clusters imply a huge number of initial structures and thus make the genetic search necessary and more effective, even though such a search is quite computationally demanding. Only a combination of different search approaches allows a consistent set of lower-energy structures to be obtained.

While low-level computations on initial geometries are carried out using the hybrid B3LYP functional in conjugation with the 6-31G(d) basis set, all selected equilibrium geometries of Si_nAl_m ($n = 1−11$, $m = 1−2$) are fully optimized using the same functional but with the larger 6-311+G(d) basis set.[64−66] In order to confirm the identity of true local minima obtained,

their harmonic vibrational frequencies are also calculated at the same level of theory.

Standard enthalpies of formation of the global minima are subsequently evaluated from the corresponding total atomization energies (TAE).[67] For this parameter, two sets of calculations are performed, including the composite G4 approach[68] and the coupled-cluster theory with complete basis set CCSD(T)/CBS. In the former approach, geometry optimizations and calculations of harmonic vibrational frequencies of clusters are carried out at the B3LYP/6-31G(2df,p) level, followed by single-point coupled-cluster theory CCSD(T) energy calculations and different additivity corrections. These methods have effectively been used to predict the thermochemical properties of a series of small boron clusters[69] and boron-doped silicon clusters.[50]

In the CCSD(T)/CBS approach used, geometrical parameters are fully optimized using the coupled-cluster CCSD(T) theory[70] along with the correlation consistent aug-cc-pVTZ basis set.[71] Single-point electronic energies are subsequently calculated using the restricted/unrestricted coupled-cluster (R/UCCSD(T)) formalism[72,73] with the aug-cc-pVnZ ($n = Q$ and 5) basis sets[71] and then extrapolated to the complete basis set limit (CBS). For simplicity, the basis sets are labeled as aVnZ. The CCSD(T) energies are extrapolated to the CBS limit energies using the expression 1:[74]

$$E(x) = E_{CBS} + B/x^3 \tag{1}$$

where $x = 4$ and 5 for the aVnZ basis with $n = Q$ and 5, respectively. Total CCSD(T) electronic energies as a function of basis set are given in Table S1 of the Supporting Information. Some other additional corrections are also included in the TAE evaluations. Core−valence corrections (ΔE_{CV}) are obtained at the CCSD(T)/aug-cc-pwCVTZ level of theory.[75] Douglas−Kroll−Hess (DKH) scalar relativistic corrections ($\Delta E_{DKH\text{-}SR}$), which account for changes due to relativistic contributions to total energies of the molecule and constituent atoms, are calculated using the spin-free, one-electron DKH Hamiltonian.[76−78] $\Delta E_{DKH\text{-}SR}$ is defined as the difference in the atomization energy between the results obtained from basis sets recontracted for DKH calculations and the atomization energy obtained with the normal valence basis set of the same quality. The DKH calculations are obtained as the differences of the results from CCSD(T)/aug-cc-pVTZ and the CCSD(T)/aug-cc-pVTZ-DK levels of theory. Finally, a spin−orbit (SO) correction of 0.21 kcal/mol for the Al atom and 0.43 kcal/mol for the Si atom are obtained from the excitation energies of Moore.[79] The total atomization energy (ΣD_0 or TAE) of a compound is given in expression 2:

$$\Sigma D_0 = \Delta E_{elec}(CBS) + \Delta E_{CV} + \Delta E_{DKH\text{-}SR} + \Delta E_{SO} - \Delta E_{ZPE} \tag{2}$$

By combining our computed ΣD_0 values determined from either the CBS or the G4 calculations, with the known experimental heats of formation at 0 K for the Al and Si elements, we can derive ΔH_f° values at 0 K for the molecules in the gas phase. In this work, we use the values at 0 K $\Delta H_f^\circ(Al) = 80.2 \pm 0.4$ kcal/mol and $\Delta H_f^\circ(Si) = 107.2 \pm 0.2$ kcal/mol.[80] We subsequently obtain the heats of formation at 298 K by following the classical thermochemical procedure.[81] The calculated heats of formation at 0 K are used to evaluate the adiabatic electron affinity (EA) and other energetic quantities. The G4 approach is used for the entire series considered, while the CBS calculations are performed only for the smaller molecules Si_nAl and Si_nAl_2 with $n = 1−3$ due to the limited computer resources.
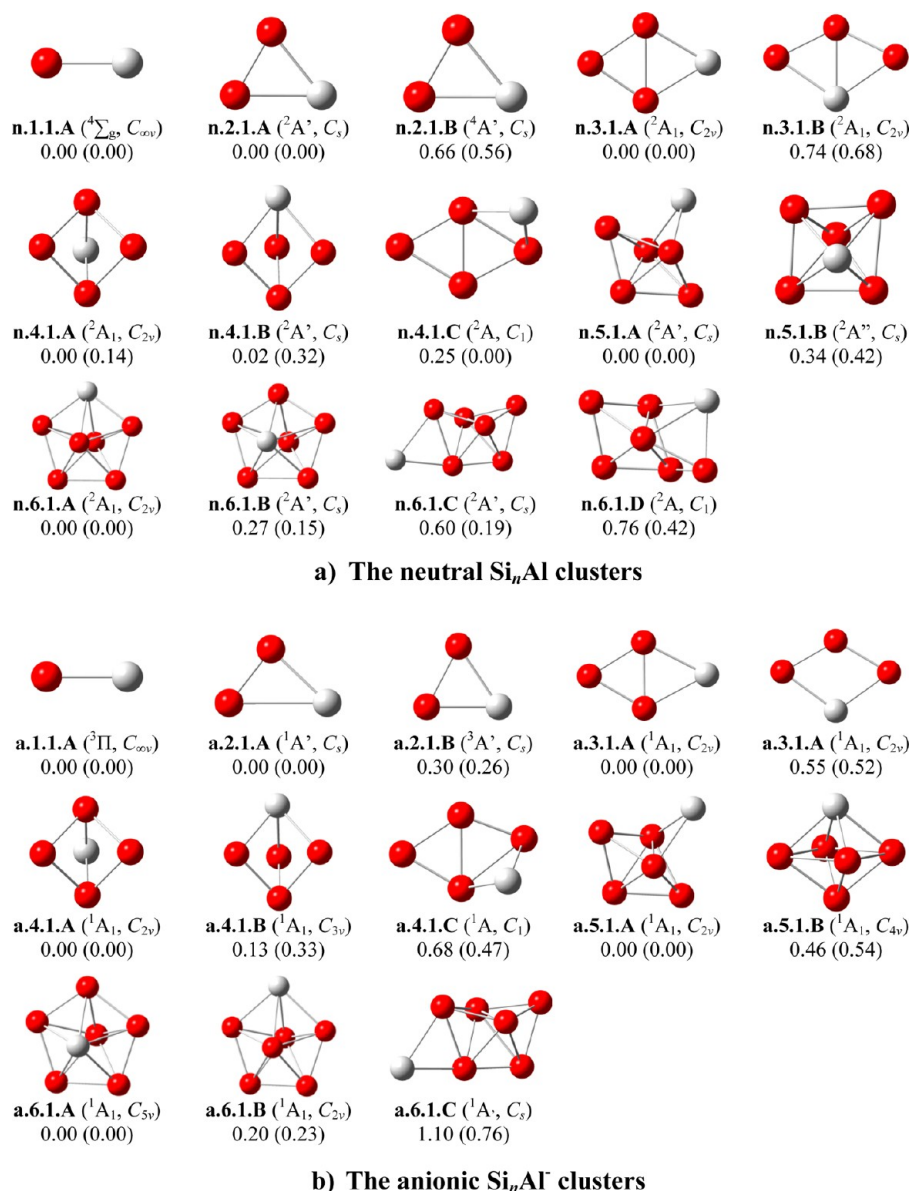
n.1.1.A ($^4\Sigma_g$, $C_{\infty v}$)   **n.2.1.A** (^{2}A', C_s)   **n.2.1.B** (^{4}A', C_s)   **n.3.1.A** (^{2}A$_1$, C_{2v})   **n.3.1.B** (^{2}A$_1$, C_{2v})
0.00 (0.00)   0.00 (0.00)   0.66 (0.56)   0.00 (0.00)   0.74 (0.68)

n.4.1.A (^{2}A$_1$, C_{2v})   **n.4.1.B** (^{2}A', C_s)   **n.4.1.C** (^{2}A, C_1)   **n.5.1.A** (^{2}A', C_s)   **n.5.1.B** (^{2}A", C_s)
0.00 (0.14)   0.02 (0.32)   0.25 (0.00)   0.00 (0.00)   0.34 (0.42)

n.6.1.A (^{2}A$_1$, C_{2v})   **n.6.1.B** (^{2}A', C_s)   **n.6.1.C** (^{2}A', C_s)   **n.6.1.D** (^{2}A, C_1)
0.00 (0.00)   0.27 (0.15)   0.60 (0.19)   0.76 (0.42)

a) The neutral Si$_n$Al clusters

a.1.1.A ($^3\Pi$, $C_{\infty v}$)   **a.2.1.A** (^{1}A', C_s)   **a.2.1.B** (^{3}A', C_s)   **a.3.1.A** (^{1}A$_1$, C_{2v})   **a.3.1.A** (^{1}A$_1$, C_{2v})
0.00 (0.00)   0.00 (0.00)   0.30 (0.26)   0.00 (0.00)   0.55 (0.52)

a.4.1.A (^{1}A$_1$, C_{2v})   **a.4.1.B** (^{1}A$_1$, C_{3v})   **a.4.1.C** (^{1}A, C_1)   **a.5.1.A** (^{1}A$_1$, C_{2v})   **a.5.1.B** (^{1}A$_1$, C_{4v})
0.00 (0.00)   0.13 (0.33)   0.68 (0.47)   0.00 (0.00)   0.46 (0.54)

a.6.1.A (^{1}A$_1$, C_{5v})   **a.6.1.B** (^{1}A$_1$, C_{2v})   **a.6.1.C** (^{1}A·, C_s)
0.00 (0.00)   0.20 (0.23)   1.10 (0.76)

b) The anionic Si$_n$Al⁻ clusters

Figure 1. Shapes, electronic states, and relative energies (ΔE, eV) of the lower-lying isomers Si$_n$Al with n = 1–6 at the (a) neutral and (b) anionic states. ΔE values are obtained using the G4 approach. Values given in brackets are from B3LYP/6-311+G(d) + ZPE computations.

3. RESULTS AND DISCUSSION

Shapes of equilibrium structures of the Si$_n$Al$_m^{0/-}$ clusters detected and their symmetry point groups and G4 relative energies are shown in Figures 1–6. The different components obtained in the CBS protocol for evaluating total atomization energies (ΣD_0) of the smaller clusters Si$_n$Al$_m^{0/-}$ (n = 1–3, m = 1–2) are given in Table 1, whereas their total CBS energies and total G4 energies for all global minima Si$_n$Al$_m^{0/-}$ are summarized in the Supporting Information. The values for heats of formation of the clusters derived from their ΣD_0 values are given in Table 2. Computed adiabatic electron affinities (EAs) of Si$_n$Al$_m$ clusters are given in Table 3, and average binding energies (E_b) are tabulated in Table 4.

3.1. Lower-Lying Isomers of Si$_n$Al$_m$ Clusters in Both Neutral and Anionic States. Because there is a large number of isomers located on the potential energy surfaces of the clusters considered, we only present in this context some lower-lying isomers whose relative energies are close to each ground

state structure (within ~1.0 eV). As for a convention, each structure described hereafter is defined by the label **x.n.m.Y** in which **x** = **n** and **a** stands for a neutral and anionic state, respectively, **n** the size of Si$_n$, **m** the size of Al$_m$, and, finally, **Y** = **A**, **B**, **C** refers to the different isomers with increasing relative energy ordering. In the following section, we briefly describe the main characteristics of the singly and doubly doped clusters, in terms of their geometry, symmetry point group, spin state, and relative energy. Concerning the energy ordering within a system, the structure labeled with the letter **A** (**x.n.m.A**) invariably refers to the lowest-lying isomer obtained from G4 calculations.

3.1.1. Singly Aluminum Doped Si$_n$Al$^{0/-}$. The main structures are displayed in Figures 1–3. There is a good agreement between our predictions and earlier reports[45,60,82] on the identification of the global minima of small-sized Si$_n$Al with n = 1–6 (Figure 1). Their main characteristics are as follows:
SiAl. The high spin state **n.1.1.A** ($^4\Sigma$) with an electronic configuration of $[1\delta^2 2\delta^2 1\pi^2 3\delta^1]$ is confirmed as the ground
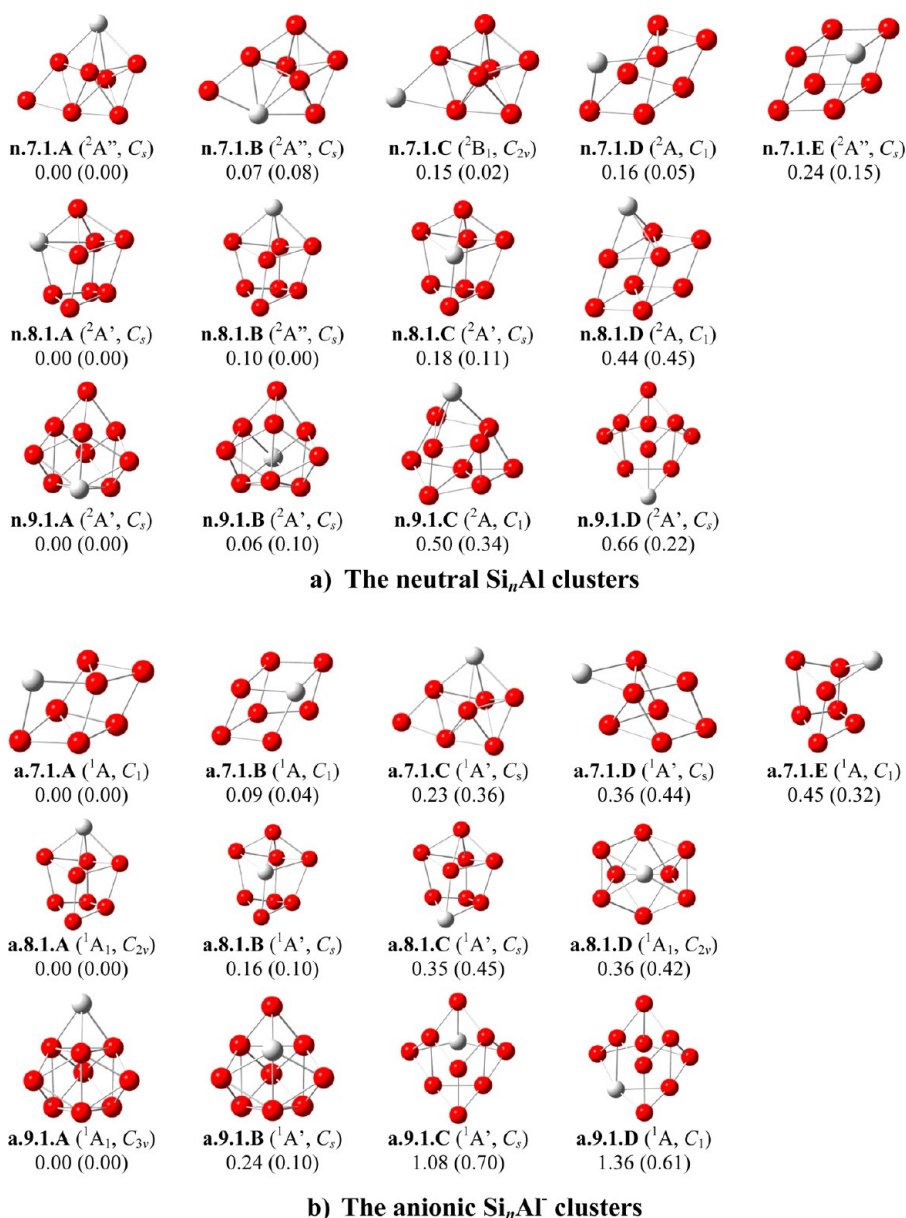
n.7.1.A (^{2}A", C_s) 0.00 (0.00)   **n.7.1.B** (^{2}A", C_s) 0.07 (0.08)   **n.7.1.C** (^{2}B$_1$, C_{2v}) 0.15 (0.02)   **n.7.1.D** (^{2}A, C_1) 0.16 (0.05)   **n.7.1.E** (^{2}A", C_s) 0.24 (0.15)

n.8.1.A (^{2}A', C_s) 0.00 (0.00)   **n.8.1.B** (^{2}A", C_s) 0.10 (0.00)   **n.8.1.C** (^{2}A', C_s) 0.18 (0.11)   **n.8.1.D** (^{2}A, C_1) 0.44 (0.45)

n.9.1.A (^{2}A', C_s) 0.00 (0.00)   **n.9.1.B** (^{2}A', C_s) 0.06 (0.10)   **n.9.1.C** (^{2}A, C_1) 0.50 (0.34)   **n.9.1.D** (^{2}A', C_s) 0.66 (0.22)

a) The neutral Si$_n$Al clusters

a.7.1.A (^{1}A, C_1) 0.00 (0.00)   **a.7.1.B** (^{1}A, C_1) 0.09 (0.04)   **a.7.1.C** (^{1}A', C_s) 0.23 (0.36)   **a.7.1.D** (^{1}A', C_s) 0.36 (0.44)   **a.7.1.E** (^{1}A, C_1) 0.45 (0.32)

a.8.1.A (^{1}A$_1$, C_{2v}) 0.00 (0.00)   **a.8.1.B** (^{1}A', C_s) 0.16 (0.10)   **a.8.1.C** (^{1}A', C_s) 0.35 (0.45)   **a.8.1.D** (^{1}A$_1$, C_{2v}) 0.36 (0.42)

a.9.1.A (^{1}A$_1$, C_{3v}) 0.00 (0.00)   **a.9.1.B** (^{1}A', C_s) 0.24 (0.10)   **a.9.1.C** (^{1}A', C_s) 1.08 (0.70)   **a.9.1.D** (^{1}A, C_1) 1.36 (0.61)

b) The anionic Si$_n$Al$^-$ clusters

Figure 2. Shapes, electronic states, and relative energies (ΔE, eV) of the lower-lying isomers Si$_n$Al with n = 7−9 at the (a) neutral and (b) anionic states. ΔE values are obtained using the G4 approach. Values given in brackets are from B3LYP/6-311+G(d) + ZPE computations.

state of the neutral diatomic, with a doublet-quartet separation gap of 1.02 eV. This electronic configuration is similar to that of Si$_2^+$. **Si$_2$Al−Si$_6$Al.** Structure **n.2.1.A** is an isosceles triangle, and **n.3.1.A** is planar. The smallest three-dimensional global minimum is found for Si$_4$Al where both structures **n.4.1.A** and **n.4.1.B** are almost degenerate with an energy gap of only 0.02 eV. Both structures are formed by replacing one Si-atom of the trigonal bipyramid Si$_5$ by one Al-atom. Similarly, both Si$_5$Al **n.5.1.A** and Si$_6$Al **n.6.1.A** are formed by substituting one Si-atom of the edge-capped trigonal bipyramid Si$_6$ and pentagonal bipyramid Si$_7$ hosts by one Al-atom, respectively.

Following attachment of one excess electron, the resulting anionic clusters Si$_n$Al$^-$ with n = 1−5 have geometries similar to their neutral counterparts (Figure 1b). Interestingly, the anionic cluster Si$_6$Al$^-$ has high symmetrical C_{5v} structure **a.6.1.A**, which is an anionic species of **n.6.1.B**. Structure **a.6.1.B**, which corresponds to an anionic state of the neutral **n.6.1.A**, turns out to be less stable with relative energy of 0.20 eV.

Si$_7$Al. There is a discrepancy between our prediction and previous reports on the identity of the Si$_7$Al ground state. Earlier studies[45,60] showed that **n.7.1.E** (C_s, ^{2}A″), which is formed by substituting one Si atom of the bicapped octahedral Si$_8$ framework by Al impurity, is the most stable isomer of Si$_7$Al. That differs from our G4 calculations that point out to the C_s structure **n.7.1.A**.

Another C_s structure **n.7.1.B** is the second isomer with only 0.07 eV higher in energy. Both isomers are formed by replacing one Si atom of the edge-capped pentagonal bipyramid of the cation Si$_8^+$ by one Al impurity.[83] Our computed results agree well with a more recent result obtained by Karamanis et al.[84]

In the anionic state, Li et al.[60] reported that **a.7.1.B** is the most stable isomer for Si$_7$Al$^-$. However, we found that both isomers **a.7.1.A** and **a.7.1.B** are almost degenerate with energy gap of only 0.09 eV. The first isomer was missed in earlier studies. Both isomers are again formed by substituting one Si atom in bicapped octahedral of the Si$_8$ host by Al dopant.
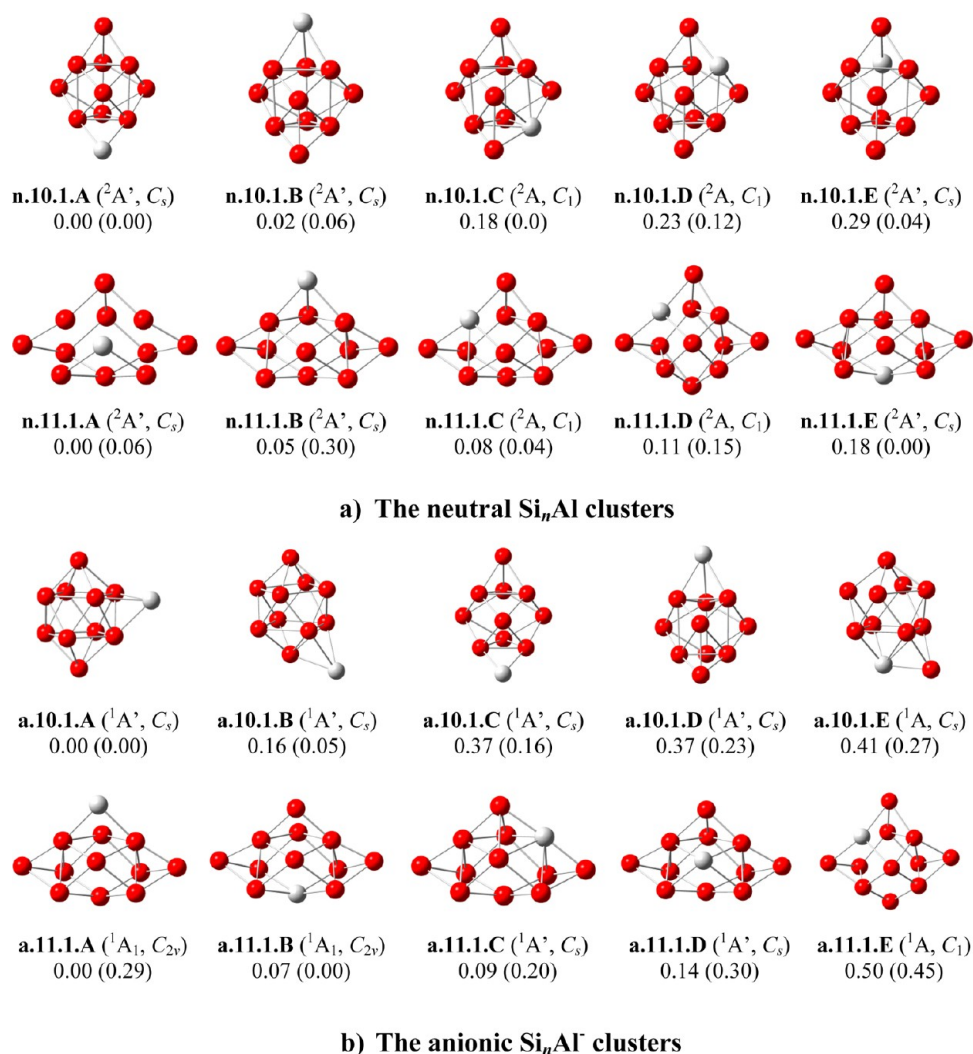
n.10.1.A (^{2}A', C_s) 0.00 (0.00) **n.10.1.B** (^{2}A', C_s) 0.02 (0.06) **n.10.1.C** (^{2}A, C_1) 0.18 (0.0) **n.10.1.D** (^{2}A, C_1) 0.23 (0.12) **n.10.1.E** (^{2}A', C_s) 0.29 (0.04)

n.11.1.A (^{2}A', C_s) 0.00 (0.06) **n.11.1.B** (^{2}A', C_s) 0.05 (0.30) **n.11.1.C** (^{2}A, C_1) 0.08 (0.04) **n.11.1.D** (^{2}A, C_1) 0.11 (0.15) **n.11.1.E** (^{2}A', C_s) 0.18 (0.00)

a) The neutral Si_nAl clusters

a.10.1.A (^{1}A', C_s) 0.00 (0.00) **a.10.1.B** (^{1}A', C_s) 0.16 (0.05) **a.10.1.C** (^{1}A', C_s) 0.37 (0.16) **a.10.1.D** (^{1}A, C_s) 0.37 (0.23) **a.10.1.E** (^{1}A, C_s) 0.41 (0.27)

a.11.1.A (^{1}A$_1$, C_{2v}) 0.00 (0.29) **a.11.1.B** (^{1}A$_1$, C_{2v}) 0.07 (0.00) **a.11.1.C** (^{1}A', C_s) 0.09 (0.20) **a.11.1.D** (^{1}A', C_s) 0.14 (0.30) **a.11.1.E** (^{1}A, C_1) 0.50 (0.45)

b) The anionic Si_nAl^- clusters

Figure 3. Shapes, electronic states, and relative energies (ΔE, eV) of the lower-lying isomers Si_nAl with $n = 10-11$ at the (a) neutral and (b) anionic states. ΔE values are obtained using the G4 approach. Values given in brackets are from B3LYP/6-311+G(d) + ZPE computations.

Si$_8$Al. Nigam et al.[45] showed that **n.8.1.B** is the most stable isomer. Our G4 calculations emphasize the global minimum character of **n.8.1.A**, being 0.10 eV below the second stable isomer **n.8.1.B**. Both isomers **n.8.1.A** and **n.8.1.B** are also formed by replacing one of Si atoms of the bicapped pentagonal bipyramid Si_9^+ framework[83] by Al.

In the negatively charged state, our G4 results indicate that **a.8.1.A** is the corresponding anion of **n.8.1.B**, whereas its isomer **a.8.1.B**, being the corresponding anion of **n.8.1.A**, is a local minimum lying 0.16 eV above **a.8.1.A**. There is thus a reversed energy ordering between isomers upon electron attachment. These results agree well with recent studies of Li et al.[60] and Karamanis et al.[84]

Si$_9$Al. The ground state **n.9.1.A** (C_s, ^{2}A') is formed by substituting one Si atom of trigonal prism of the tetra-capped trigonal prism cage of Si_{10}[85] by Al dopant. G4 calculations result in a near degeneracy of both **n.9.1.B** and **n.9.1.B** with a gap of only 0.06 eV.

In the anionic state, a higher symmetry structure **a.9.1.A** (C_{3v}, ^{1}A$_1$) is determined. Both lowest-lying isomers **a.9.1.A** and **a.9.1.B** (at 0.24 eV above **a.9.1.A**) have a tetra-capped trigonal prism Si_{10} framework. Other anionic structures are much less stable.

Si$_{10}$Al. According to B3LYP calculations, four neutral isomers **n.10.1.A**, **n.10.1.B**, **n.10.1.C**, and **n.10.1.E** that exhibit the same penta-capped trigonal prism framework of pure Si_{11}[45] are energetically degenerate within an energy range of 0.06 eV. At the G4 level, however, the isomers **n.10.1.C** and **n.10.1.E** are now 0.18 and 0.29 eV higher in energy than **n.10.1.A**, respectively. For their part, **n.10.1.A** and **n.10.1.B** have the same energy content (a tiny gap of 0.02 eV) and both thus constitute the dual global minima of Si_{10}Al. These predictions are in good agreement with those of Karamanis et al.[84]

There is again a discrepancy between our predictions and earlier studies for the ground state of the anion Si_{10}Al$^-$. A previous study[60] showed that **a.10.1.D**, which is the corresponding anion of **n.10.1.B**, is the most stable form. Our G4 calculations indicate that **a.10.1.A** is at 0.16 eV below **a.10.1.B**. Both lowest-lying isomers are formed by capping an Al atom on a face of a bicapped squared antiprism cage of the pure Si_{10}^{-2} dianion.[86]

Si$_{11}$Al. Our B3LYP calculations agree with Li et al.[60] that **n.11.1.E** is the most stable form, while both isomers **n.11.1.C** and **n.11.1.A** are energetically degenerate with only 0.04 and 0.06 eV less stable than **n.11.1.E**, respectively. Conversely, taking G4 results, **n.11.1.A** is now 0.18 eV more stable than
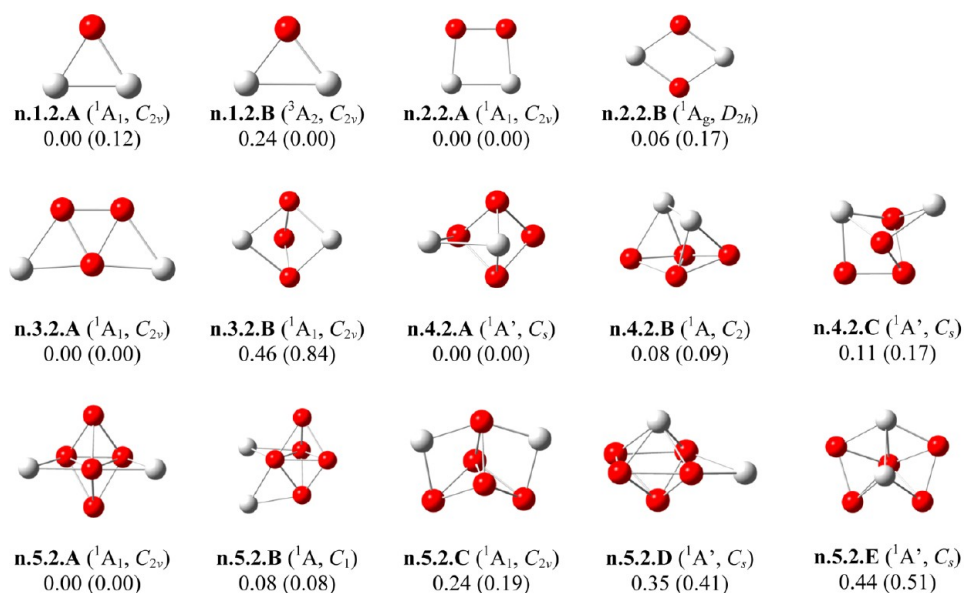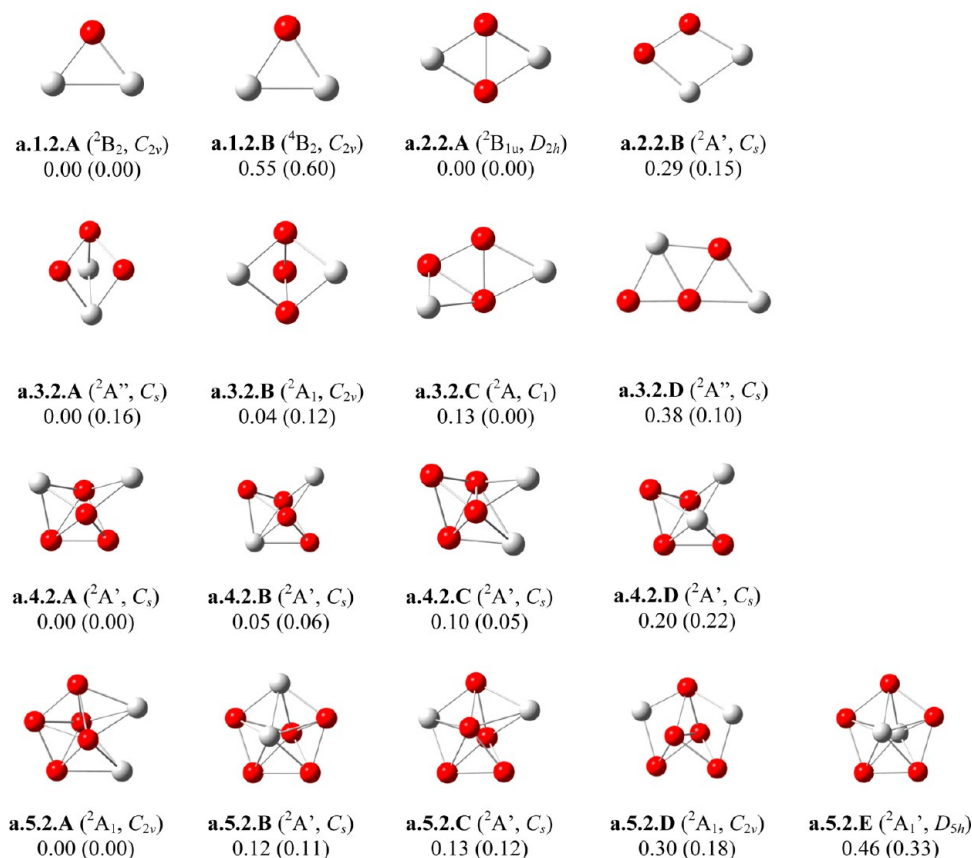
n.1.2.A ($^1A_1$, C_{2v})
0.00 (0.12)

n.1.2.B ($^3A_2$, C_{2v})
0.24 (0.00)

n.2.2.A ($^1A_1$, C_{2v})
0.00 (0.00)

n.2.2.B (^1A_g, D_{2h})
0.06 (0.17)

n.3.2.A ($^1A_1$, C_{2v})
0.00 (0.00)

n.3.2.B ($^1A_1$, C_{2v})
0.46 (0.84)

n.4.2.A ($^1A'$, C_s)
0.00 (0.00)

n.4.2.B (^1A, C_2)
0.08 (0.09)

n.4.2.C ($^1A'$, C_s)
0.11 (0.17)

n.5.2.A ($^1A_1$, C_{2v})
0.00 (0.00)

n.5.2.B (^1A, C_1)
0.08 (0.08)

n.5.2.C ($^1A_1$, C_{2v})
0.24 (0.19)

n.5.2.D ($^1A'$, C_s)
0.35 (0.41)

n.5.2.E ($^1A'$, C_s)
0.44 (0.51)

a) The neutral Si$_n$Al$_2$ clusters

a.1.2.A ($^2B_2$, C_{2v})
0.00 (0.00)

a.1.2.B ($^4B_2$, C_{2v})
0.55 (0.60)

a.2.2.A ($^2B_{1u}$, D_{2h})
0.00 (0.00)

a.2.2.B ($^2A'$, C_s)
0.29 (0.15)

a.3.2.A ($^2A''$, C_s)
0.00 (0.16)

a.3.2.B ($^2A_1$, C_{2v})
0.04 (0.12)

a.3.2.C (^2A, C_1)
0.13 (0.00)

a.3.2.D ($^2A''$, C_s)
0.38 (0.10)

a.4.2.A ($^2A'$, C_s)
0.00 (0.00)

a.4.2.B ($^2A'$, C_s)
0.05 (0.06)

a.4.2.C ($^2A'$, C_s)
0.10 (0.05)

a.4.2.D ($^2A'$, C_s)
0.20 (0.22)

a.5.2.A ($^2A_1$, C_{2v})
0.00 (0.00)

a.5.2.B ($^2A'$, C_s)
0.12 (0.11)

a.5.2.C ($^2A'$, C_s)
0.13 (0.12)

a.5.2.D ($^2A_1$, C_{2v})
0.30 (0.18)

a.5.2.E ($^2A_1'$, D_{5h})
0.46 (0.33)

b) The anionic Si$_n$Al$_2^-$ clusters

Figure 4. Shapes, electronic states, and relative energies (ΔE, eV) of the lower-lying isomers Si$_n$Al$_2$ with $n = 1-5$ at the (a) neutral and (b) anionic states. ΔE values are obtained using the G4 method. Values given in brackets are from B3LYP/6-311+G(d) + ZPE computations.

n.11.1.E. Both **n.11.1.B** and **n.11.1.C** are again energetically degenerate with only 0.05 and 0.08 eV higher than the lowest-energy isomer, respectively. A reason for such a close energy is that these low-lying isomers can all be formed by replacement

of one Si atom of hexa-capped trigonal prism Si$_{12}^+$ cage[45] by the Al dopant.

For the anions, Li et al.[60] reported **a.11.1.C** as the most stable Si$_{11}$Al$^-$ shape. Our G4 results do not concur with

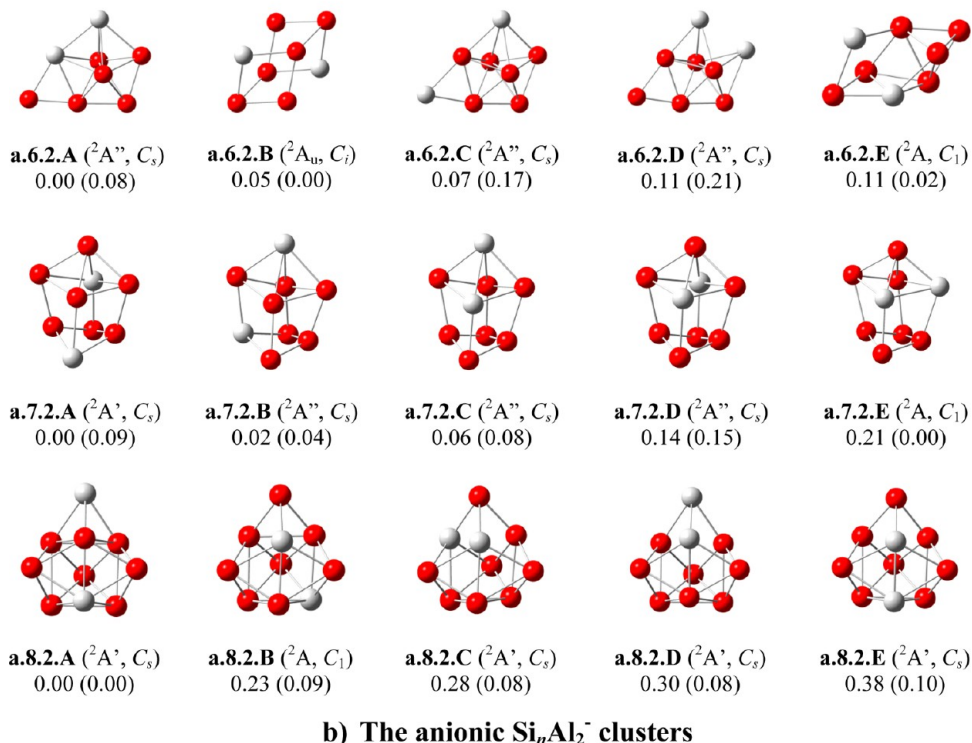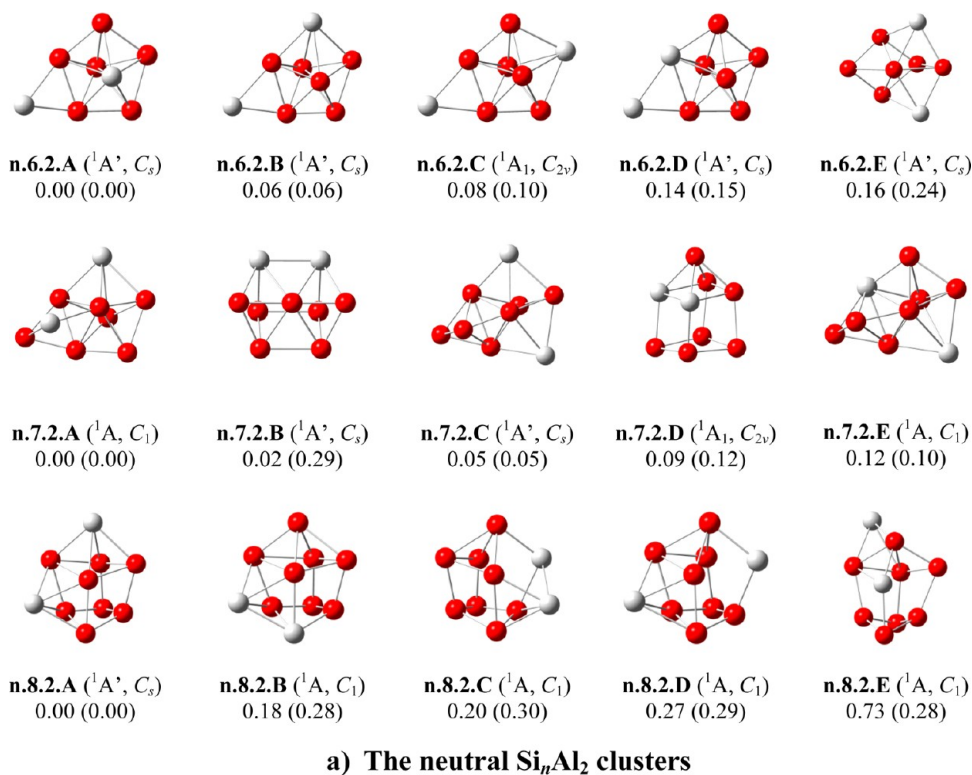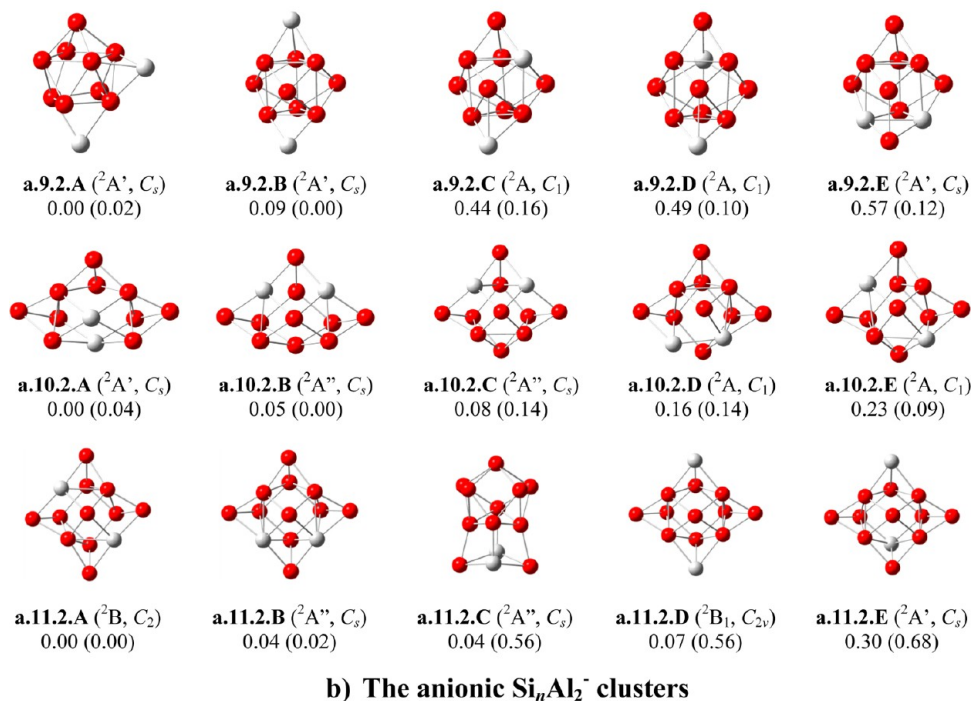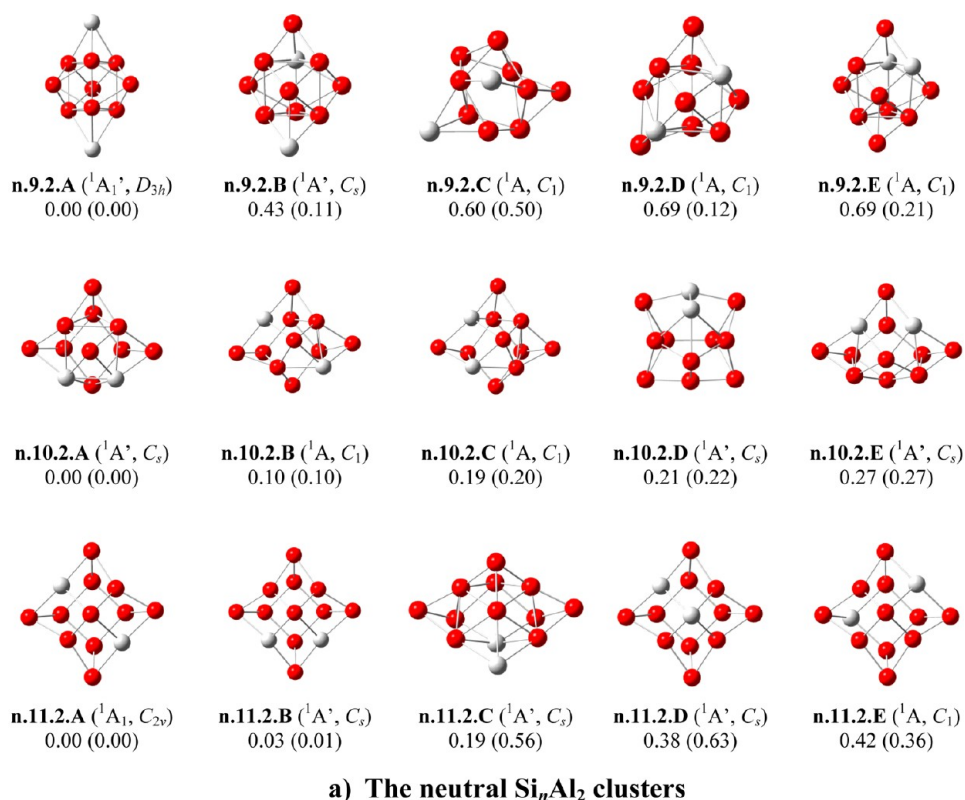**n.6.2.A** (^{1}A', C_s)   **n.6.2.B** (^{1}A', C_s)   **n.6.2.C** (^{1}A$_1$, C_{2v})   **n.6.2.D** (^{1}A', C_s)   **n.6.2.E** (^{1}A', C_s)
0.00 (0.00)   0.06 (0.06)   0.08 (0.10)   0.14 (0.15)   0.16 (0.24)

n.7.2.A (^{1}A, C_1)   **n.7.2.B** (^{1}A', C_s)   **n.7.2.C** (^{1}A', C_s)   **n.7.2.D** (^{1}A$_1$, C_{2v})   **n.7.2.E** (^{1}A, C_1)
0.00 (0.00)   0.02 (0.29)   0.05 (0.05)   0.09 (0.12)   0.12 (0.10)

n.8.2.A (^{1}A', C_s)   **n.8.2.B** (^{1}A, C_1)   **n.8.2.C** (^{1}A, C_1)   **n.8.2.D** (^{1}A, C_1)   **n.8.2.E** (^{1}A, C_1)
0.00 (0.00)   0.18 (0.28)   0.20 (0.30)   0.27 (0.29)   0.73 (0.28)

a) The neutral Si$_n$Al$_2$ clusters

a.6.2.A (^{2}A", C_s)   **a.6.2.B** (^{2}A$_u$, C_i)   **a.6.2.C** (^{2}A", C_s)   **a.6.2.D** (^{2}A", C_s)   **a.6.2.E** (^{2}A, C_1)
0.00 (0.08)   0.05 (0.00)   0.07 (0.17)   0.11 (0.21)   0.11 (0.02)

a.7.2.A (^{2}A', C_s)   **a.7.2.B** (^{2}A", C_s)   **a.7.2.C** (^{2}A", C_s)   **a.7.2.D** (^{2}A", C_s)   **a.7.2.E** (^{2}A, C_1)
0.00 (0.09)   0.02 (0.04)   0.06 (0.08)   0.14 (0.15)   0.21 (0.00)

a.8.2.A (^{2}A', C_s)   **a.8.2.B** (^{2}A, C_1)   **a.8.2.C** (^{2}A', C_s)   **a.8.2.D** (^{2}A', C_s)   **a.8.2.E** (^{2}A', C_s)
0.00 (0.00)   0.23 (0.09)   0.28 (0.08)   0.30 (0.08)   0.38 (0.10)

b) The anionic Si$_n$Al$_2^-$ clusters

Figure 5. Shapes, electronic states, and relative energies (ΔE, eV) of the lower-lying isomers Si$_n$Al$_2$ with n = 6−8 at the (a) neutral and (b) anionic states. ΔE values are obtained using the G4 approach. Values given in brackets are from B3LYP/6-311+G(d) + ZPE computations.

this finding and instead favor **a.11.1.A**, which is the corresponding anion of **n.11.1.B**. Again, the anionic forms **a.11.1.B** and **a.11.1.C** are only 0.07 and 0.09 eV higher in energy, respectively.

It is apparent that substitution by Al at different Si centers of a pure Si cluster leads to multiple mixed isomers with comparable energy content. Such a pattern is in particular reinforced in the anions where both Al$^-$ anion and Si atom are isoelectronic.

3.1.2. Doubly Aluminum Doped Si$_n$Al$_m^{0/-}$ *with* n = 1−11 *and* m = 2. Their structural evolution can be seen in Figures 4 (n = 1−5), 5 (n = 6−8), and 6 (n = 9−11).

n.9.2.A ($^1A_1'$, D_{3h})
0.00 (0.00)

n.9.2.B ($^1A'$, C_s)
0.43 (0.11)

n.9.2.C (^1A, C_1)
0.60 (0.50)

n.9.2.D (^1A, C_1)
0.69 (0.12)

n.9.2.E (^1A, C_1)
0.69 (0.21)

n.10.2.A ($^1A'$, C_s)
0.00 (0.00)

n.10.2.B (^1A, C_1)
0.10 (0.10)

n.10.2.C (^1A, C_1)
0.19 (0.20)

n.10.2.D ($^1A'$, C_s)
0.21 (0.22)

n.10.2.E ($^1A'$, C_s)
0.27 (0.27)

n.11.2.A ($^1A_1$, C_{2v})
0.00 (0.00)

n.11.2.B ($^1A'$, C_s)
0.03 (0.01)

n.11.2.C ($^1A'$, C_s)
0.19 (0.56)

n.11.2.D ($^1A'$, C_s)
0.38 (0.63)

n.11.2.E (^1A, C_1)
0.42 (0.36)

a) The neutral Si_nAl_2 clusters

a.9.2.A ($^2A'$, C_s)
0.00 (0.02)

a.9.2.B ($^2A'$, C_s)
0.09 (0.00)

a.9.2.C (^2A, C_1)
0.44 (0.16)

a.9.2.D (^2A, C_1)
0.49 (0.10)

a.9.2.E ($^2A'$, C_s)
0.57 (0.12)

a.10.2.A ($^2A'$, C_s)
0.00 (0.04)

a.10.2.B ($^2A''$, C_s)
0.05 (0.00)

a.10.2.C ($^2A''$, C_s)
0.08 (0.14)

a.10.2.D (^2A, C_1)
0.16 (0.14)

a.10.2.E (^2A, C_1)
0.23 (0.09)

a.11.2.A (^2B, C_2)
0.00 (0.00)

a.11.2.B ($^2A''$, C_s)
0.04 (0.02)

a.11.2.C ($^2A''$, C_s)
0.04 (0.56)

a.11.2.D ($^2B_1$, C_{2v})
0.07 (0.56)

a.11.2.E ($^2A'$, C_s)
0.30 (0.68)

b) The anionic $Si_nAl_2^-$ clusters

Figure 6. Shapes, electronic states, and relative energies (ΔE, eV) of the lower-lying isomers Si_nAl_2 with $n = 9-11$ at the (a) neutral and (b) anionic states. ΔE values are obtained using the composite G4 method. Values given in brackets are from B3LYP/6-311+G(d) + ZPE computations.

SiAl$_2$. For the triatomic species (Figure 4), at the B3LYP level, the high spin triangle **n.1.2.B** ($^3A_2$, C_{2v}) is the neutral ground state being 0.12 eV lower in energy than the same shape isomer but with a closed-shell electronic configuration **n.1.2.A** ($^1A_1$, C_{2v}). This is at variance with our G4 calculations that point out a reversed energy ordering in favor of **n.1.2.A**, with

energy gap of 0.24 eV below **n.1.2.B**. For the charged state, both B3LYP and G4 methods agree with each other confirming the doublet triangle **a.1.2.A** ($^2B_2$, C_{2v}) as the ground state. The higher spin isomer **a.1.2.B** ($^4B_2$, C_{2v}) is significantly less stable than **a.1.2.A**, being at 0.55 (G4) and 0.60 eV (B3LYP) higher in energy than **a.1.2.A**.

Table 1. Total Atomization Energies (ΣD_0, TAE, kcal/mol) of Si_nAl_m Clusters ($n = 1-3$, $m = 1-2$) and Different Components of CCSD(T)/CBS Computations

structure	state	ΔCBS^a	$E_{ZPE}{}^b$	$\Delta E_{CV}{}^c$	$\Delta E_{SR}{}^d$	$\Delta E_{SO}{}^e$	ΣD_0 (TAE)
a.1.1.A	$^3\Pi$	90.30	0.60	−0.14	−0.34	−0.64	88.57
n.1.1.A	$^4\Sigma_g$	58.80	0.54	0.19	−0.15	−0.64	57.66
a.2.1.A	$^1A'$	200.42	1.41	0.16	−0.65	−1.07	197.45
n.2.1.A	$^2A'$	148.25	1.29	0.38	−0.52	−1.07	145.76
a.3.1.A	$^1A_1$	306.50	2.69	0.68	−0.90	−1.50	302.08
n.3.1.A	$^2A_1$	249.02	2.73	0.90	−0.67	−1.50	245.02
a.1.2.A	$^2B_2$	165.27	1.22	−0.09	−0.63	−0.85	162.47
n.1.2.A	$^1A_1$	119.09	1.40	−0.06	−0.55	−0.85	116.23
a.2.2.A	$^2B_{1u}$	268.30	2.50	0.36	−0.87	−1.28	264.00
n.2.2.A	$^1A_1$	221.92	2.56	0.79	−0.56	−1.28	218.30
a.3.2.A	$^2A''$	356.67	3.39	1.02	−1.08	−1.71	351.51
n.3.2.A	$^1A_1$	307.91	3.12	1.39	−0.77	−1.71	303.71

[a]Extrapolated by using eq 1 with the aVQZ and aV5Z basis sets. [b]Zero-point energies taken from CCSD(T) harmonic vibrational frequencies. [c]Core−valence corrections obtained with the aug-cc-pwCVTZ basis set at CCSD(T) optimized geometries. [d]Scalar relativistic corrections based on CCSD(T)-DK/aug-cc-pVTZ-DK calculations and expressed relative to the CCSD(T) results without DK corrections. [e]Corrections due to the incorrect treatment of the atomic asymptotes as an average of spin multiplets. Values based on Moore's Tables, ref 79.

Si_2Al_2. For the tetraatomic cluster (Figure 4), the lowest-lying isomers in both neutral and anionic states possess planar structure. The low spin **n.2.2.A** ($^1A_1$, C_{2v}) and the higher symmetry **n.2.2.B** (^1A_g, D_{2h}) are again energetically quasi-degenerate with a gap of only 0.06 eV (this energy gap being 0.17 eV at the B3LYP level). **a.2.2.A**, which is actually the anionic state of **n.2.2.B**, becomes the ground state with 0.29 eV (G4) more stable than **a.2.2.B** as a consequence of energy ordering reversal upon electron attachment.

Si_3Al_2. For the pentaatomic molecules (Figure 4), the neutral isomer **n.3.2.A** ($^1A_1$, C_{2v}), in which two Al atoms add on two edges of the Si_3 triangle, is the lowest-lying isomer, and the second isomer **n.3.2.B** lies at 0.46 eV higher in energy. In the anion state, **a.3.2.C**, the corresponding anion of **n.3.2.A**, is the lowest-lying isomer at the B3LYP level. Our G4 results show a higher stability for **a.3.2.A**, being 0.16 eV lower than **a.3.2.C**, but **a.3.2.B** is found at only 0.04 eV below **a.3.2.A**. Both **a.3.2.A** and **a.3.2.B** have the trigonal bipyramid shape of the pure Si_5 cluster in which two Si positions are now occupied by two Al atoms.

Si_4Al_2. **n.4.2.A** ($^1A'$, C_s) is formed by substituting one Si atom of the trigonal bipyramid framework of Si_5 by an Al dopant, whereas the other Al is added on an edge of it (Figure 4). The singlet **n.4.2.B** (^1A, C_2), formed by a similar way, has an energy separation of only 0.09 eV.

In the anionic state, two lowest-lying isomers **a.4.2.A** and **a.4.2.B** also have a tiny energy gap of 0.05 eV. The isomer **a.4.2.C** is also a stable structure being only 0.1 eV below **a.4.2.A**. Interestingly, all lower-lying anions $Si_4Al_2{}^-$ possess an edge-capped trigonal bipyramid Si_6 host in which both Al atoms differently occupy two Si positions of the pure cluster.

Si_5Al_2. The low spin neutral **n.5.2.A** ($^1A_1$, C_{2v}) and the next isomer **n.5.2.B** (^1A, C_1) are formed by adding two Al atoms on two edges of the pure trigonal bipyramid Si_5 framework. In other words, they both have the shape of the pure Si_6 counterpart in which one Si position is changed by an Al atom whereas the other Al adds on one of its edges (Figure 4). As a consequence, both structures are close in energy (0.08 eV). In the charged state, **a.5.2.A** arises from the swapping of two Si atoms by two Al atoms in a pentagonal bipyramid Si_7 form.

The other local minima are in this case at most 0.5 eV above **a.5.2.A**.

Si_6Al_2. The same degeneracy pattern is again verified for this system, either in the neutral or the charged state (Figure 5). The neutrals **n.6.2.A** ($^1A'$, C_s), **n.6.2.B** ($^1A'$, C_s), and **n.6.2.C** ($^1A_1$, C_{2v}) are separated from each other by only 0.06−0.08 eV (G4). Remarkably the four lowest-lying isomers of neutral Si_6Al_2 have a pentagonal bipyramid Si_7 form in which the first Al atom replaces one Si, and the second Al is capping on a pentagon edge.

In the charged state, a competition emerges between **a.6.2.A** ($^2A''$, C_s) and **a.6.2.B** (^2A_u, C_i) (Figure 5). According to B3LYP, **a.6.2.B** is 0.08 eV lower in energy than **a.6.2.A**, but G4 results indicate a reversed energy ordering even though **a.6.2.A** is only 0.05 eV below **a.6.2.B**. Both structures practically exist as the degenerate ground state of the anion $Si_6Al_2{}^-$. The isomer **a.6.2.A** possesses a capped pentagonal bipyramid structure of the $Si_8{}^+$ cation,[83] produced by a double Al substitution, whereas **a.6.2.B** exhibits the bicapped octahedral shape of neutral Si_8[45] in which two Si atoms are also substituted by two Al. Isomer **a.6.2.C**, being the corresponding anion of **n.6.2.B**, is again at 0.07 eV above **a.6.2.A** (G4 values).

Si_7Al_2. The singlet neutral **n.7.2.A** (^1A, C_1) is characterized by the capped pentagonal bipyramid of the cation $Si_8{}^+$ in which the first Al atom substitutes a Si atom in the pentagon and the remaining Al caps on its face (Figure 5). Besides, G4 results also point out similar energy locations for **n.7.2.A**, **n.7.2.B** ($^1A'$, C_s), and **n.7.2.C** ($^1A'$, C_s) (a gap of 0.02−0.05 eV; G4 and B3LYP levels).

All the five lower-lying isomeric anions $Si_7Al_2{}^-$ derived from the same bicapped pentagonal bipyramidal block of the bare Si_9 cluster thus possess similar energy content. According to G4 results, three isomers **a.7.2.A** ($^2A'$, C_s), **a.7.2.B** ($^2A''$, C_s), and **a.7.2.C** ($^2A''$, C_s) are located within a tiny gap of only 0.02 and 0.06 eV. Although **a.7.2.E** is found to be the lowest-lying structure at the B3LYP level, it is becomes now at 0.21 eV above **a.7.2.A** using the G4 method. There is thus a spectrum of global minima that feature the same 3D shape but with different positions of the dopants.

Si_8Al_2. The neutral **n.8.2.A** ($^1A'$, C_s) involves an Al capping on a surface of the pure neutral Si_9 and a substitution of the

Table 2. Heats of Formation at 0 K $[\Delta H_f (0\ K)]$ and 298 K $[\Delta H_f (298\ K)]$ (kcal/mol) of Si_nAl_m ($n = 1-11$, $m = 1-2$) in Both Neutral and Anionic States Obtained Using G4 and CCSD(T)/CBS Calculations

structure	$\Delta H_f (0\ K)$		$\Delta H_f (298\ K)$	
	G4	CBS	G4	CBS
a.1.1.A	100.8	98.8	101.2	99.2
n.1.1.A	127.9	129.7	128.3	130.1
a.2.1.A	94.3	97.2	94.9	97.7
n.2.1.A	146.6	148.8	147.3	149.5
a.3.1.A	96.6	99.7	97.3	100.4
n.3.1.A	155.2	156.8	155.8	157.4
a.4.1.A	106.2		106.6	
n.4.1.A	178.1		179.1	
a.5.1.A	97.4		98.3	
n.5.1.A	165.5		166.5	
a.6.1.A	106.0		106.9	
n.6.1.A	181.7		182.7	
a.7.1.A	140.4		141.7	
n.7.1.A	206.0		207.5	
a.8.1.A	138.6		140.1	
n.8.1.A	219.9		221.4	
a.9.1.A	126.6		128.1	
n.9.1.A	217.8		219.5	
a.10.1.A	155.8		157.9	
n.10.1.A	229.0		231.1	
a.11.1.A	177.1		179.2	
n.11.1.A	259.5		261.5	
a.1.2.A	103.4	105.1	103.7	105.4
n.1.2.A	147.3	151.4	147.5	151.6
a.2.2.A	107.0	110.8	107.4	111.2
n.2.2.A	153.8	156.5	154.2	156.9
a.3.2.A	125.2	130.5	126.0	130.6
n.3.2.A	175.6	178.3	176.6	178.7
a.4.2.A	110.7		111.4	
n.4.2.A	169.7		170.5	
a.5.2.A	121.6		122.8	
n.5.2.A	181.9		183.2	
a.6.2.A	143.9		145.1	
n.6.2.A	193.2		194.3	
a.7.2.A	156.3		157.8	
n.7.2.A	215.5		217.0	
a.8.2.A	148.8		150.3	
n.8.2.A	209.7		211.3	
a.9.2.A	152.7		154.6	
n.9.2.A	205.9		207.7	
a.10.2.A	186.9		188.7	
n.10.2.A	248.0		249.6	
a.11.2.A	197.9		199.6	
n.11.2.A	259.0		260.6	

Table 3. Adiabatic Electronic Affinities (EA, eV) of Si_nAl_m ($n = 1-11$, $m = 1-2$) Using G4 and CCSD(T)/CBS Calculations

	Si_nAl		Si_nAl_2	
n	G4	CBS	G4	CBS
1	1.17	1.34	1.90	2.00
2	2.27	2.24	2.03	1.98
3	2.54	2.47	2.18	2.07
4	3.11		2.56	
5	2.95		2.61	
6	3.28		2.14	
7	2.85		2.57	
8	3.52		2.64	
9	3.96		2.31	
10	3.17		2.65	
11	3.57		2.65	

Table 4. Average Binding Energies (E_b, eV) of Si_nAl_m ($n = 1-11$, $m = 1-2$) Using G4 Calculations

n	Si_nAl	Si_nAl^-	Si_nAl_2	$Si_nAl_2^-$
1	1.29	1.20	1.74	1.92
2	2.14	2.45	2.40	2.57
3	2.67	2.97	2.66	2.82
4	2.87	3.22	3.03	3.23
5	3.26	3.52	3.19	3.37
6	3.36	3.63	3.31	3.41
7	3.39	3.57	3.35	3.49
8	3.46	3.70	3.51	3.63
9	3.59	3.85	3.62	3.71
10	3.64	3.81	3.56	3.67
11	3.61	3.80	3.60	3.70

isomer **n.9.2.B** ($^1A'$, C_s). Nevertheless, both structures are generated by a similar way: by capping an Al atom at different faces of the tetra-capped trigonal prism Si_{10} and by substituting a Si atom by the other Al atom at different positions (Figure 6). The remaining isomers are now much less stable, being at least 0.60 eV (G4) higher in energy than **n.9.2.A**.

In contrast to the neutrals, an energetic degeneracy persists in the charged state. The two lowest-lying anionic forms **a.9.2.A** ($^2A'$, C_s) and **a.9.2.B** ($^2A'$, C_s) are in fact separated by only 0.02 eV in favor of the latter (B3LYP). G4 results, however, point out a reversed energy ordering at the expense of **a.9.2.B**, but with a small gap of 0.09 eV with respect to **a.9.2.A**. The latter contains a bicapped squared antiprism Si skeleton of the pure dianionic Si_{10}^{2-} structure.[86] As usual, one capped Si atom is substituted by an Al dopant, whereas the other Al caps on a face of the cage. The second stable **a.9.2.B** and the remaining lower-lying isomers are, as expected, generated by substituting two Si positions in the pure Si_{11} framework by both Al dopants.

$Si_{10}Al_2$. n.10.2.A ($^1A'$, C_s) is calculated at 0.10 and 0.20 eV lower than **n.10.2.B** and **n.10.2.C**, respectively (Figure 6). These lowest-lying isomers are all generated by a double substitution of two Si positions from the ground state of the hexa-capped trigonal prism of the pure Si_{12}^+ cation.[45] A competition in relative stability apparently occurs between both anionic isomers **a.10.2.A** and **a.10.2.B**. At the B3LYP/6-311+G(d) level, **a.10.2.B** ($^2A''$, C_s) is 0.04 eV more stable than **a.10.2.A** ($^2A'$, C_s). G4 results again show a reversed energy ordering in that **a.10.2.A** is 0.05 eV lower in energy than **a.10.2.B**. As in the $Si_9Al_2^-$ case, the energetic degeneracy is not lifted yet for the anions $Si_{10}Al_2^-$.

remaining Al atom (Figure 5). In this system, the usual degeneracy is removed. Three isomers **n.8.2.B**, **n.8.2.C**, and **n.8.2.D**, formed by the same way, are now 0.30 eV above **n.8.2.A**. In the same vein, the energy gap between anionic isomers equally tends to increase, with **a.8.2.A** ($^2A'$, C_s) being 0.23 eV (G4) more stable than the second isomer **a.8.2.B** (^2A, C_1). All lower-lying anionic isomers of $Si_8Al_2^-$ are constructed from a tetra-capped trigonal prism structure of the pure Si_{10} with both Al atoms substituting two Si ones.

Si_9Al_2. The high symmetry neutral **n.9.2.A** ($^1A_1'$, D_{3h}) is apparently stabilized, being now 0.43 eV below the second

In both global minima structures, two Si atoms on the Si_{12}^+ skeleton are substituted by two Al dopants. G4 calculations also indicate that the third isomer **a.10.2.C** is only 0.08 eV higher in energy than **a.10.2.A**, being thus practically competing with the former.

Si₁₁Al₂. Surprisingly, an energetic degeneracy comes back for this system (Figure 6). The separation between both isomers **n.11.2.A** ($^1A_1$, C_{2v}) and **n.11.2.B**($^1A'$, C_s) amounts now only to 0.03 eV (G4). Both isomers contain a Si hepta-capped trigonal prism similar to the ground state of the Si_{13}^+ cation,[45] with substitution of both Al atoms at different Si positions. The isomer **n.11.2.C**, formed by adding an Al atom on the Si_{12}^+ stable geometry and substituting one Si atom in it by the other Al, is a low-energy local minimum at 0.19 eV above **n.11.2.A**.

The anion $Si_{11}Al_2^-$ holds the energetic trend in having two very close-lying isomers **a.11.2.A** (having the shape of the neutral **n.11.2.A**) and **a.11.2.B** (having the shape of **n.11.2.B**) in which the former is only 0.05 eV below the latter (Figure 6). Calculated G4 results also emphasize two other energetically higher but degenerate structures **a.11.2.C** and **a.11.2.D**.

3.2. Equilibrium Growth Sequence of the Si_nAl_m Clusters. On the basis of the structural features of the most stable isomers identified above, the growth pattern of the clusters Si_nAl_m with $n = 1-11$ and $m = 1-2$ can be established considering the following findings.

Because the Al element has one valence electron less than the Si, Al is isoelectronic with Si^+, and Al^- with Si. Thus, in a singly doped neutral Si_nAl, the Al atom favors substitution at a Si position of silicon framework of the isoelectronic cation Si_{n+1}^+. In other words, the ground state structure of a neutral Si_nAl cluster can be derived from the pure cation Si_{n+1}^+.

Similarly, a Si_nAl^- anion has the Al atom substituted into a Si position of the ground state structure of the neutral Si_{n+1}. The most stable structure of the anion $Si_{10}Al^-$, however, has an Al atom being added on the face of the dianionic Si_{10}^{2-} framework. This can be understood by the high thermodynamic stability of the latter dianion.

The growth patterns of both neutral Si_nAl and anionic Si_nAl^- systems are found to be comparable to those of the isovalent Si_nB and Si_nB^-, respectively, reported in our earlier study,[50] with $n = 1-7$. The essential difference between Si_nAl and Si_nB clusters resides in the fact that the Al–Si bond lengths in the mixed framework are much longer than the B–Si counterparts. Because of the shorter bond length, the B-impurity can be more easily encapsulated into a Si_n cage, even at a smaller size ($n \geq 8$) than the Al-dopant. Endohedral doping occurs much earlier in the boron series.

In the doubly doped neutral Si_nAl_2 clusters, with $n = 1-9$, each mixed cluster can be regarded as a direct derivative of a Si_{n+1} counterpart in which one Si atom is actually substituted by an Al dopant. Such an operation leads to a ground state structure similar to the cation Si_{n+1}^+. The other Al atom is usually added on an edge, or a face, of the existing cluster. In the larger neutral $Si_{10}Al_2$ and $Si_{11}Al_2$ ground states, they are basically made by simple substitution of two Si atoms in the corresponding cation Si_{12}^+ and Si_{13}^+ cages, respectively, by two Al dopants.

For the negatively charged state, the $Si_nAl_2^-$ anions also contain the cationic Si_{n+2}^+ skeletons in which two Si positions are substituted by two Al dopants. Again, such a similarity in growth pattern can be rationalized by the lack of one electron in the outermost orbital of Al atom, which makes them isoelectronic. However, the anion $Si_9Al_2^-$ represents an exception to this sequence. The lowest-lying structure of $Si_9Al_2^-$ includes one Al atom substituting a Si position of the dianionic Si_{10}^{2-} cage, and the other Al capping on its face, due to the high thermodynamic stability of the dianion counterpart.

It can be seen that the $Si_nAl_m^q$ clusters tend to be formed by a substituting motif rather than a capping motif. As a matter of fact, geometries of $Si_nAl_m^q$ and Si_{n+m}^{q+m} are similar, due to the smaller valence electron number, by one unit, of each Al atom. For singly doped silicon clusters Si_nAl^q, the Al dopant looks to avoid high coordination position. Except for the anion Si_6Al^- where Al has a maximum coordination number of 5, the Al in other stable species prefers occupation of positions having lower coordination numbers.

3.3. Thermochemical Properties. Calculated results are summarized in Table 2. At the first glance, a reasonable agreement between both sets of CCSD(T)/CBS and G4 results emerges. The enthalpies of formation at 0 K (ΔH^0_f) obtained using CCSD(T)/CBS are found to be slightly larger than those obtained by the composite G4, except for the diatomic SiAl. The difference varies in the range of 1.6−5.3 kcal/mol for the species considered (Table 2).

The adiabatic electron affinities (EAs) are obtained from the energy difference between the neutrals Si_nAl_m and their corresponding $Si_nAl_m^-$ anions. As expected for relative quantities, the EA values given in Table 3 also confirm an overall agreement between both theoretical approaches. The maximum difference between two sets of values amounts to 0.17 eV for EAs of Si_nAl, and 0.11 eV for EAs of Si_nAl_2. These differences of energetic properties between both G4 and CCSD(T)/CBS methods can be understood from the ways of determining the geometries, as well as of computing single-point electronic energies. Let us remind that, in our CCSD(T)/CBS protocol, geometries are optimized at the CCSD(T)/aug-cc-pVTZ level, whereas the G4 uses B3LYP/6-31G(2df,p) optimizations. As far as we are aware, experimental or previous theoretical data are not actually available for these mixed clusters.

3.4. Relative Stability of Clusters. In order to probe the inherent stability of the clusters considered, the average binding energies (E_b) of clusters are examined. The average binding energies (E_b) can conventionally be defined as follows (eqs 3−6):

$$E_b(Si_nAl) = [nE(Si) + E(Al) - E(Si_nAl)]/(n + 1) \qquad (3)$$

$$E_b(Si_nAl^-) = [(n - 1)E(Si) + E(Si^-) + E(Al) \\ - E(Si_nAl^-)]/(n + 1) \qquad (4)$$

$$E_b(Si_nAl_2) = [nE(Si) + 2E(Al) - E(Si_nAl_2)]/(n + 2) \qquad (5)$$

$$E_b(Si_nAl_2) = [(n - 1)E(Si) + E(Si^-) + 2E(Al) \\ - E(Si_nAl^-)]/(n + 2) \qquad (6)$$

where $E(Al)$, $E(Si)$, $E(Si^-)$ are the total energies of the Al atom, Si atom, and the anion Si^-, respectively. For their part, $E(Si_nAl)$, $E(Si_nAl^-)$, $E(Si_nAl_2)$, and $E(Si_nAl_2^-)$ are total energies of the neutral Si_nAl, anionic Si_nAl^-, neutral Si_nAl_2, and anionic $Si_nAl_2^-$ structures, respectively. All these energies are obtained from G4 calculations. While the E_b values are given in Table 4, plots illustrating their evolution are depicted in Figure 7.

The E_b values increase with increasing cluster sizes. For neutral Si_nAl clusters, the $Si_{10}Al$ reveals the highest E_b value as compared to those of the remaining singly doped species. At the anionic state, Si_9Al^- presents with the highest E_b value that indicates its high thermodynamical stability. This finding is in
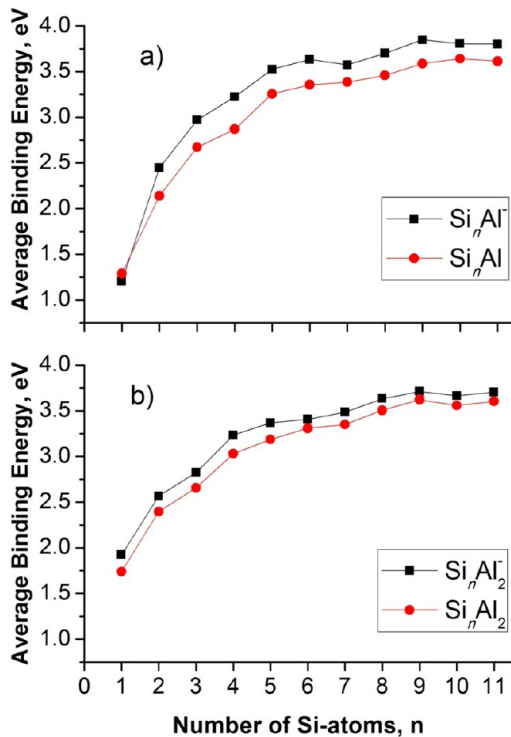
Figure 7. Average binding energy (E_b, eV) of the $Si_nAl_m^{/0/-}$ ($n = 1-11$, $m = 1-2$) clusters using the composite G4 method.

agreement with the fact that the isoelectronic Si_{10} is a quite stable pure Si cluster. For Si_nAl_2 clusters, the Si_9Al_2 in both neutral and anionic states consistently attain the maximum peaks in the E_b plots.

3.5. Dissociation Energies. To evaluate further the thermodynamic stability, dissociation energies (D_e) for the various fragmentation channels of both singly and doubly aluminum doped silicon clusters considered are determined. Results calculated from total G4 energies are shown in Table 5. The dissociation energies of the neutrals Si_nAl for the Si-elimination channel (1) $Si_nAl \rightarrow Si_{n-1}Al + Si$ turn out to be larger than those for the Al-loss channel (2) $Si_nAl \rightarrow Si_n + Al$.

Similar observations are found for the negatively charged species that the anionic Si_nAl^- clusters tend to be fragmented generating one Al element plus a smaller anion Si_n^- along the fragmentation channel (5).

For doubly doped neutral Si_nAl_2 clusters, dissociation energies for Al-loss channels (8) $Si_nAl_2 \rightarrow Si_nAl + Al$ are invariably smaller than those for Si-elimination pathways (7) $Si_nAl_2 \rightarrow Si_{n-1}Al_2 + Si$, and for the diatomic aluminum Al_2-loss route (9) $Si_nAl_2 \rightarrow Si_n + Al_2$.

Similarly, the anions $Si_nAl_2^-$ follow preferential fragmentation to form one Al plus a smaller anion Si_nAl^- along the channel (12) $Si_nAl_2^- \rightarrow Si_nAl^- + Al$.

3.6. Jellium Electron Shell Model (JSM). As for a rationalization of the relative stabilities of Si_nAl clusters, we reexamine their MO pictures under the viewpoint of the jellium

Table 5. Dissociation Energies (D_e, kcal/mol) for Various Fragmentation Channels of Si_nAl_m ($n = 1-11$, $m = 1-2$) from G4 Calculations[a]

	Si_nAl					
	neutrals		anions			
n	$D_e(1)$	$D_e(2)$	$D_e(3)$	$D_e(4)$	$D_e(5)$	$D_e(6)$
1	59.5	59.5	77.3	55.5	55.5	77.3
2	88.4	73.5	113.7	109.7	73.1	116.5
3	98.6	73.6	104.8	126.1	78.7	122.8
4	84.3	52.5	97.6	125.1	74.0	115.0
5	119.8	73.7	116.1	156.8	84.2	132.5
6	91.1	58.5	98.6	135.7	84.6	124.9
7	82.9	40.0	72.9	117.4	61.3	96.3
8	93.3	65.7	108.9	143.5	87.9	137.6
9	109.3	69.1	119.3	169.4	109.9	151.0
10	96.0	48.5	77.9	138.1	67.5	112.3
11	76.7	56.6	85.9	128.0	80.1	129.7
	Si_nAl_2					
	neutrals			anions		
n	$D_e(7)$	$D_e(8)$	$D_e(9)$	$D_e(10)$	$D_e(11)$	$D_e(12)$	$D_e(13)$	$D_e(14)$	$D_e(15)$
1	88.1	60.8	88.1	63.8	100.9	77.6	95.3	100.9	94.8
2	100.7	73.1	114.4	72.6	116.5	67.5	110.6	108.4	124.0
3	85.4	59.9	101.2	57.9	104.7	51.6	100.9	98.2	114.4
4	113.1	88.6	108.9	90.6	141.0	75.8	138.3	117.5	130.8
5	95.0	63.9	105.4	65.2	124.2	56.0	114.8	108.0	128.5
6	95.9	68.7	95.0	53.9	114.1	42.3	108.7	94.7	107.2
7	84.9	70.7	78.4	63.7	112.9	64.2	120.5	93.3	100.5
8	113.0	90.4	123.8	83.6	142.8	70.0	141.9	125.7	147.6
9	110.9	92.1	128.9	72.3	133.1	54.1	136.0	131.8	145.0
10	65.2	61.2	77.5	41.9	95.2	49.2	113.0	84.5	101.4
11	96.2	80.7	105.1	65.1	126.2	59.4	132.4	107.3	129.0

[a](1) $Si_nAl \rightarrow Si_{n-1}Al + Si$; (2) $Si_nAl \rightarrow Si_n + Al$; (3) $Si_nAl^- \rightarrow Si_{n-1}Al^- + Si$; (4) $Si_nAl^- \rightarrow Si_{n-1}Al + Si^-$; (5) $Si_nAl^- \rightarrow Si_n^- + Al$; (6) $Si_nAl^- \rightarrow Si_n + Al^-$; (7) $Si_nAl_2 \rightarrow Si_{n-1}Al_2 + Si$; (8) $Si_nAl_2 \rightarrow Si_nAl + Al$; (9) $Si_nAl_2 \rightarrow Si_n + Al_2$; (10)$Si_nAl_2^- \rightarrow Si_{n-1}Al_2^- + Si$; (11) $Si_nAl_2^- \rightarrow Si_{n-1}Al_2 + Si^-$; (12) $Si_nAl_2^- \rightarrow Si_nAl^- + Al$; (13) $Si_nAl_2^- \rightarrow Si_nAl + Al^-$; (14) $Si_nAl_2^- \rightarrow Si_n^- + Al_2$; (15) $Si_nAl_2^- \rightarrow Si_n + Al_2^-$.

shell model (JSM).[87] The total density of states (DOS) of a molecular system can be considered as an energy spectrum of its molecular orbitals (MOs). The partial density of states (pDOS) is computed only from relevant atomic orbitals and thereby shows the composition of the MOs involved.

This simple model is successfully applied to interpret the stability motif of different types of doped silicon clusters in our recent studies.[49−52] Accordingly, the valence electrons are supposed to be freely itinerant in a simple mean-field potential formed by the nuclei of atoms and core electrons, the valence electrons fill the hydrogen-like orbitals following the pattern of orbitals as $[1S^2 1P^6 1D^{10} 2S^2 1F^{14} 2P^6 1G^{18} 2D^{10}...]$, etc. Within this model, the number of electrons of 8, 20, 34, 40, 56, and 68 emerge as the *magic numbers* that actually correspond to a complete filling of the successive shell electrons.

In this context, and as for a typical example, we examine the valence electronic configuration of the anionic cluster Si_9Al^- (cf. Figure 8a) due to its enhanced stability. In order to provide

effectively correspond to the same energy sequence of the electronic shell model $[1S^2 1P^6 1D^{10} 2S^2 1F^{14} 2P^6]$.

In this case, the DOSs of both Si_9Al^- and Si_{10} structures show many similarities as they have the same C_{3v} point group. The pDOS plots also reveal that the MOs of Si_9Al^- are mainly composed of the s-AOs and p-AOs of Si-atoms, whereas the contribution of s-AOs and p-AOs is negligible to split the subshells.

Let us note a relationship between the DOS of Si_9Al^- and the DOS of the isovalent Si_9B^- ($^1A_1'$, D_{3h}), which was reported in our recent study.[50] Both anionic structures contain the same silicon Si_9 cage in which the B dopant is encapsulated but the Al dopant caps on its face. The boron anion Si_9B^- also has 40 valence electrons and its DOS features are quite similar to that of Si_9Al^-, and generally, the electronic structure of both anions Si_9Al^- and Si_9B^- satisfies the electron shell configuration of $[1S^2 1P^6 1D^{10} 2S^2 2P^6 1F^{14}]$; this basically makes them enhanced stability species with a *magic number of 40 valence electrons*.

4. CONCLUDING REMARKS

In the present theoretical study, geometrical and electronic structures of the aluminum doped silicon Si_nAl_m clusters, with $n = 1-11$ and $m = 1-2$, in both neutral and anionic states were determined using quantum chemical methods. The global energy minima of the clusters considered are identified on the basis of G4 energies. Total atomization energies, enthalpies of formation, and thermochemical properties including electron affinity, average binding energy, and dissociation energies are predicted for the first time using the high accuracy G4 and CCSD(T)/CBS methods.

In most of the sizes investigated, two or more lowest-lying isomers of each size are calculated to be energetically degenerate (G4 values). Substitution of Si atoms at different positions of a corresponding pure silicon clusters by Al dopants invariably leads to a spectrum of distinct binary structures but with similar shape and comparable energy content. Such an energetic degeneracy persists in the larger cluster sizes, in particular for the anions.

The growth sequence for singly and doubly aluminum doped silicon clusters can be established as follows: (i) in the neutral Si_nAl, the Al dopant prefers substitution into one of the Si positions of the pure cation Si_{n+1}^+. Formally, an anion Si_nAl^- can formally be produced from the neutral Si_{n+1} by substitution of any Si atom by the Al impurity; (ii) the growth pattern of both neutrals Si_nAl and anions Si_nAl^- is similar to the structural evolution of their isovalent counterparts, namely, the neutrals Si_nB and anions Si_nB^-, respectively. Having longer Al−Si bond lengths than the B−Si distances, the Al impurity cannot easily intrude inside the corresponding Si_n cage (for up to $n \geq 8$) such as the specific characteristic of the B dopant; (iii) the doubly doped neutral Si_nAl_2 clusters possess the shape of their pure Si_{n+1}^+ counterparts. One Al dopant replaces a Si atom of the latter, and the other Al dopant adds on an edge or a face. This differs from the growth pattern of the anions $Si_nAl_2^-$ where both Al atoms simply substitute two Si centers of a Si_{n+2}^+ framework; and (iv) the neutral $Si_{10}Al_2$ and $Si_{11}Al_2$ clusters and their anions emerge as interesting exceptions in which the Al dopants behave differently. This can be understood from characteristics and stability of the relevant pure Si clusters.

Figure 8. Total (DOS) and partial (pDOS) densities of state of (a) Si_9Al^- and (b) Si_{10}.

with an answer to the question of why Si_9Al^- is getting high stability, the neutral cluster Si_{10} ($^1A_1$, C_{3v}), which is known for its high thermodynamic stability, is taken as a reference (cf. Figure 8b). Both structures in fact contain 40 valence electrons. The Si_9Al^- anion possesses an orbital configuration of $(1a_1)^2(1e)^4(2a_1)^2(2e)^4(3a_1)^2(3e)^4(4a_1)^2(4e)^4(1a_2)^2(5a_1)^2(5e)^4$ $(6a_1)^2(6e)^4(7a_1)^2$, and the neutral Si_{10} ($^1A_1$, C_{3v}) pure cluster has an orbital configuration of $(1a_1)^4(1e)^4(2a_1)^2(2e)^8(3a_1)^4-$ $(3e)^4(1a_2)^2(4a_1)^2(5e)^8(6a_1)^2$. Both orbital configurations

■ ASSOCIATED CONTENT

ⓢ Supporting Information

Tables contain the single-point electronic energies obtained at the CCSD(T)/auc-cc-pVnZ levels (n = Q, 5) and their CBS
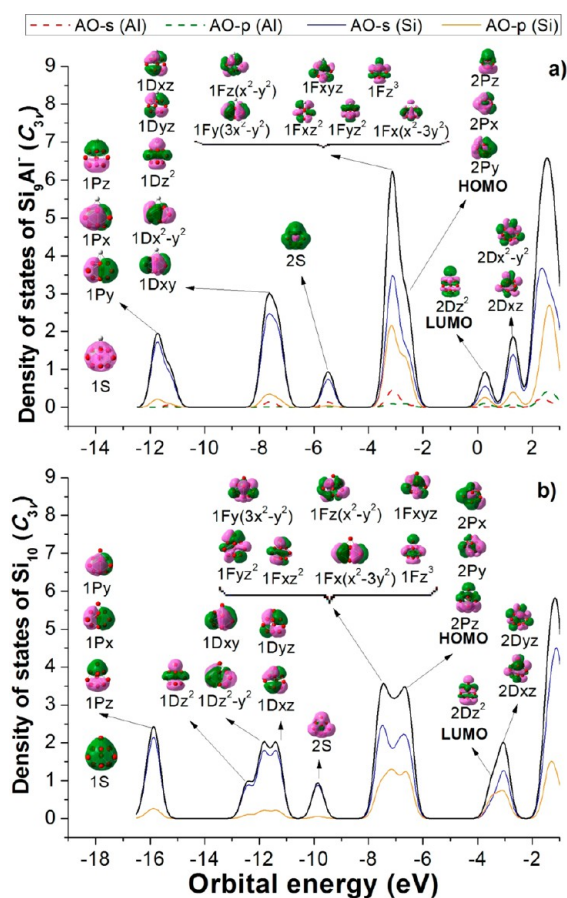
values. Cartesian coordinates of low-lying isomers $Si_nAl^{0/-}$ (B3LYP geometries obtained within G4 calculations). Total G4 energies and TAEs of $Si_nAl^{-/0}$. Total G4 energies of pure silicon clusters $Si_n^{0/\mp}$. This material is available free of charge via the Internet at http://pubs.acs.org.

■ **AUTHOR INFORMATION**

Corresponding Author

*(M.T.N.) Fax: +32-16-327992. E-mail: minh.nguyen@chem.kuleuven.be.

Notes

The authors declare no competing financial interest.

■ **REFERENCES**

(1) Ferrando, R.; Jellinek, J.; Johnston, R. L. Nanoalloys: From Theory to Applications of Alloy Clusters and Nanoparticles. *Chem. Rev.* **2008**, *108*, 845–910.

(2) (a) Raghavachari, K.; Logovinsky, V. Structure and Bonding in Small Silicon Clusters. *Phys. Rev. Lett.* **1985**, *55*, 2853–2856. (b) Brown, W. L.; Freeman, R. R.; Raghavachari, K.; Schluter, M. Covalent Group IV Atomic Clusters. *Science* **1987**, *235*, 860–865. (c) Honea, E. C.; Ogura, A.; Murray, C. A.; Raghavachari, K.; Sprenger, W. O.; Jarrold, M. F.; Brown, W. L. Raman Spectra of Size-Selected Silicon Clusters and Comparison with Calculated Structures. *Nature* **1993**, *366*, 42–44.

(3) Pacchioni, G.; Koutecký, J. Silicon and Germanium Clusters. A Theoretical Study of Their Electronic Structures and Properties. *J. Chem. Phys.* **1986**, *84*, 3301–3310.

(4) Veldeman, N.; Gruene, P.; Fielicke, A.; Claes, P.; Ngan, V. T.; Nguyen, M. T.; Lievens, P. Endohedrally Doped Silicon Clusters. In *Handbook of Nanophysics. Clusters and Fullerenes*; Sattler, K. D., Ed.; CRC Press: Boca Raton, FL, 2010; Chapter 5.

(5) Cheshnovsky, O.; Yang, S. H.; Pettiette, C. L.; Craycraft, M. J.; Liu, Y.; Smalley, R. E. Ultraviolet Photoelectron Spectroscopy of Semiconductor Clusters: Silicon and Germanium. *Chem. Phys. Lett.* **1987**, *138*, 119–124.

(6) Winstead, C. B.; Paukstis, S. J.; Gole, J. L. What Is the Ionization Potential of Silicon Dimer? *Chem. Phys. Lett.* **1995**, *237*, 81–85.

(7) Claes, P.; Ngan, V. T.; Haertelt, M.; Lyon, J. T.; Fielicke, A.; Nguyen, M. T.; Lievens, P.; Janssens, E. The Structures of Neutral Transition Metal Doped Silicon Clusters, Si_nX (n = 6–9; X = V, Mn). *J. Chem. Phys.* **2013**, *138*, 194301.

(8) Röthlisberger, U.; Andreoni, W.; Parrinello, M. Structure of Nanoscale Silicon Clusters. *Phys. Rev. Lett.* **1994**, *72*, 665–668.

(9) Li, S.; Van Zee, R. J.; Weltner, W.; Raghvachari, K. Si_3–Si_7. Experimental and Theoretical Infrared Spectra. *Chem. Phys. Lett.* **1995**, *243*, 275–280.

(10) Ho, K. M.; Shvartsburg, A. A.; Pan, B.; Lu, Z. Y.; Wang, C. Z.; Wacker, J. G.; Fye, J. L.; Brown, W. L. Structures of Medium-Sized Silicon Clusters. *Nature* **1998**, *392*, 582–585.

(11) Shvartsburg, A. A.; Liu, B.; Jarrold, M. F.; Ho, K. M. Modeling Ionic Mobilities by Scattering on Electronic Density Isosurfaces: Application to Silicon Cluster Anions. *J. Chem. Phys.* **2000**, *112*, 4517–4526.

(12) (a) Zhu, X.; Zeng, X. C. Structures and Stabilities of Small Silicon Clusters: Ab initio molecular-orbital calculations of Si_7–Si_{11}. *J. Chem. Phys.* **2003**, *118*, 3558–3570. (b) Xu, H. G.; Wu, M. M.; Zhang, Z. G.; Yuan, J. Y.; Sun, Q.; Zheng, W. J. Photoelectron Spectroscopy and Density Functional Calculations of $CuSi_n^-$ (n = 4–18) Clusters. *J. Chem. Phys.* **2012**, *136*, 104308.

(13) Hellmann, W.; Hennig, R. G.; Goedecker, S.; Umrigar, C. J.; Delley, B.; Lenosky, T. Questioning the Existence of a Unique Ground-State Structure for Si Clusters. *Phys. Rev. B* **2007**, *75*, 085411–085415.

(14) Beck, S. M. Studies of Silicon Cluster–Metal Atom Compound Formation in a Supersonic Molecular Beam. *J. Chem. Phys.* **1987**, *87*, 4233–4234.

(15) Claes, P.; Janssens, E.; Ngan, V. T.; Gruene, P.; Lyon, J. T.; Harding, D. J.; Fielicke, A.; Nguyen, M. T.; Lievens, P. Structural Identification of Caged Vanadium Doped Silicon Clusters. *Phys. Rev. Lett.* **2011**, *107*, 173401.

(16) (a) Li, G. L.; Ma, W. L.; Gao, A. M.; Chen, H. Y.; Finlow, D.; Li, Q. S. Density Functional Theory Studies of Charged, Copper-Doped, Small Silicon Clusters, $CuSi_n^+/CuSi_n^-$ (n = 1–7). *J. Theor. Comput. Chem.* **2012**, *11*, 185–196. (b) Liu, T. G.; Zhao, G. F.; Wang, Y. X. Structural, Electronic and Magnetic Properties of $GdSi_n$ (n = 1–17) Clusters: A Density Functional Study. *Phys. Lett. A* **2011**, *375*, 1120–1127.

(17) Ziella, D. H.; Caputo, M. C.; Provasi, P. F. Study of Geometries and Electronic Properties of $AgSi_n$ Clusters Using DFT/TB. *Int. J. Quantum Chem.* **2011**, *111*, 1680–1693.

(18) Cheshnovsky, O.; Yang, S. J.; Pettiette, C. L.; Craycraft, M. J.; Liu, Y.; Smalley, R. E. Ultraviolet Photoelectron Spectroscopy of Semiconductor Clusters: Silicon and Germanium. *Chem. Phys. Lett.* **1987**, *138*, 119.

(19) (a) Ye, J. Z.; Li, B. X. First-Principles Study on Mixed $Si_{10-n}N_n$ (n = 0–10) Clusters. *J. Phys. B* **2010**, *405*, 1461–1465. (b) Fan, H. W.; Yang, J. C.; Lu, W.; Ning, H. M.; Zhang, Q. C. Structures and Electronic Properties of Beryllium Atom Encapsulated in $Si_n^{(0,-1)}$ (n = 2–10) Clusters. *J. Phys. Chem. A* **2010**, *114*, 1218–1223.

(20) (a) Xu, H. G.; Zhang, Z. G.; Feng, Y. A.; Zheng, W. J. Photoelectron Spectroscopy and Density-Functional Study of $Sc_2Si_n^-$ (n = 2–6) Clusters. *Chem. Phys. Lett.* **2010**, *498*, 22–26. (b) Xu, H. G.; Zhang, Z. G.; Feng, Y.; Yuan, J. Y.; Zhao, Y. C.; Zheng, W. J. Vanadium-Doped Small Silicon Clusters: Photoelectron Spectroscopy and Density-Functional Calculations. *Chem. Phys. Lett.* **2010**, *487*, 204–208.

(21) De Haeck, J.; Bhattacharyya, S.; Le, H. T.; Debruyne, D.; Tam, N. M.; Ngan, V. T.; Janssens, E.; Nguyen, M. T.; Lievens, P. Ionization Energies and Structures of Lithium Doped Silicon Clusters. *Phys. Chem. Chem. Phys.* **2012**, *14*, 8542–8550.

(22) He, J. G.; Wu, K. C.; Sa, R. J.; Li, Q. H.; Wei, Y. Q. (Hyper)polarizabilities and Optical Absorption Spectra of MSi_{12} Clusters (M = Sc–Zn): A Theoretical Study. *Chem. Phys. Lett.* **2010**, *490*, 132–137.

(23) Ngan, V. T.; Janssens, E.; Claes, P.; Lyon, J. T.; Fielicke, A.; Nguyen, M. T.; Lievens, P. High Magnetic Moments in Manganese Doped Silicon Clusters. *Chem.—Eur. J.* **2012**, *18*, 15788–15793.

(24) (a) Zdetsis, A. D.; Koukaras, E. N.; Garoufalis, C. S. A Parallel Study of Ni@Si_{12} and Cu@Si_{12} Nanoclusters. *J. Math. Chem.* **2009**, *46*, 971–980. (b) Zdetsis, A. D. A New Class of Silicon-Carbon Clusters: A Full Study of the Hydrogenated $Si_nC_2H_2$, n = 3,4,5, Clusters in Comparison with Their Isoelectronic Carboranes $C_2B_nH_{n+2}$. *J. Chem. Phys.* **2008**, *128*, 184305. (c) Zdetsis, A. D. High-Stability Hydrogenated Silicon–carbon Clusters: A Full Study of $Si_2C_2H_2$ in Comparison to Si_2C_2, $C_2B_2H_4$, and Other Similar Species. *J. Phys. Chem. A* **2008**, *112*, 5712–5719. (d) Zdetsis, A. D. Bonding and Structural Characteristics of Zn-, Cu-, and Ni-Encapsulated Si Clusters: Density-Functional Theory Calculations. *Phys. Rev. B* **2007**, *75*, 085409.

(25) (a) Robles, R.; Khanna, S. N. Magnetism in Assembled and Supported Silicon Endohedral Cages: First-Principles Electronic Structure Calculations. *Phys. Rev. B* **2009**, *80*, 115414. (b) Robles, R.; Khanna, S. N. Stable $T_2Si_n(T$ = Fe,Co,Ni,$1 \leq n \leq 8$) Cluster Motifs. *J. Chem. Phys.* **2009**, *130*, 164313.

(26) (a) Li, J. R.; Wang, G. H.; Yao, C. H.; Mu, Y. W.; Wan, J. G.; Han, M. Structures and Magnetic Properties of Si_nMn (n = 1–15) Clusters. *J. Chem. Phys.* **2009**, *130*, 164514–. (b) Li, B. X.; Wang, G. Y.; Ding, W. F.; Ren, X. J.; Ye, J. Z. First-Principles Study on Mixed

6880

dx.doi.org/10.1021/jp405280c | *J. Phys. Chem. A* 2013, 117, 6867–6882

$Si_{n-1}N$ (n = 1−19) Clusters. *Phys. B: Condens. Matter* **2009**, *404*, 1679−1685.

(27) (a) Quenau, V.; Todorov, E.; Sevov, S. C. Synthesis and Structure of Isolated Silicon Clusters. *J. Am. Chem. Soc.* **1998**, *120*, 3263−3264. (b) Fischer, S. A.; Madrid, A. B.; Isborn, C. M.; Prezhdo, P. V. Multiple Exciton Generation in Small Si Clusters: A High-Level, Ab Initio Study. *J. Phys. Chem. Lett.* **2010**, *1*, 232−237.

(28) Lan, Y.-Z.; Feng, Y.-L. Comparative Study on the Geometric and Energetic Properties, Absorption Spectra, and Polarizabilities of Charged and Neutral $Cu@Si_n$ Clusters (n = 9−14). *Phys. Rev. A* **2009**, *79*, 033201.

(29) Hao, D. S.; Liu, J. R.; Wu, W. G.; Yang, J. C. Study on Structures and Electron Affinities of Small Potassium−Silicon Clusters Si_nK (n = 2−8) and Their Anions with Gaussian-3 Theory. *Theor. Chem. Acc.* **2009**, *124*, 431−437.

(30) Grubisic, A.; Ko, Y. J.; Wang, H.; Bowen, K. H. Photoelectron Spectroscopy of Lanthanide−Silicon Cluster Anions $LnSi_n^-$ (3 ≤ n ≤ 13; Ln = Ho, Gd, Pr, Sm, Eu, Yb): Prospect for Magnetic Silicon-Based Clusters. *J. Am. Chem. Soc.* **2009**, *131*, 10783−10790.

(31) Lin, L. H.; Yang, J. C.; Ning, H. M.; Hao, D. S.; Fan, H. W. Silicon−Sodium Binary Clusters Si_nNa (n < 10) and Their Anions: Structures, Thermochemistry, and Electron Affinities. *J. Mol. Struct.* **2008**, *851*, 197−206.

(32) Li, X.; Wang, H.; Grubisic, A.; Wang, D.; Bowen, K. H.; Jackson, M.; Kiran, B. Heteroborane Analogs of Silicon Clusters: Experimental and Theoretical Studies on Bi_2Si_5 and $Bi_2Si_5^-$. *J. Chem. Phys.* **2008**, *129*, 134309.

(33) Koyasu, K.; Atobe, J.; Furuse, S.; Nakajima, A. Anion Photoelectron Spectroscopy of Transition Metal- and Lanthanide Metal-Silicon Clusters: MSi_n^- (n = 6−20). *J. Chem. Phys.* **2008**, *129*, 214301.

(34) Hossain, D.; Pittman, C. U.; Gwaltney, S. R. Structures and Stabilities of Copper Encapsulated within Silicon Nano-Clusters: $Cu@Si_n$ (n = 9−15). *Chem. Phys. Lett.* **2008**, *451*, 93−97.

(35) Hao, D.; Liu, J.; Yang, J. A Gaussian-3 Theoretical Study of Small Silicon−Lithium Clusters: Electronic Structures and Electron Affinities of Si_nLi^- (n = 2−8). *J. Phys. Chem. A* **2008**, *112*, 10113−10119.

(36) Guo, L.-J.; Zhao, G.-F.; Gu, Y.-Z.; Liu, X.; Zeng, Z. Density-Functional Investigation of Metal-Silicon Cage Clusters MSi_n (M = Sc, Ti, V, Cr, Mn, Fe, Co, Ni, Cu, Zn; n = 8−16). *Phys. Rev. B* **2008**, *77*, 195417.

(37) Gruene, P.; Fielicke, A.; Meijer, G.; Janssens, E.; Ngan, V. T.; Nguyen, M. T.; Lievens, P. Tuning the Geometric Structure by Doping Silicon Clusters. *ChemPhysChem* **2008**, *9*, 811−816.

(38) Dkhissi, A. Evaluation of Exchange-Correlation Functionals in Comparison to B3LYP for the Description of Silicon and Cu-Doped Silicon Clusters. *Int. J. Quantum Chem.* **2008**, *108*, 996−1003.

(39) Cao, Y.; Hockendorf, R. F.; Beyer, M. K. Gas Phase Ion Chemistry of Gold−Silicon Clusters. *ChemPhysChem* **2008**, *9*, 1383−1386.

(40) Cao, T. T.; Feng, X. J.; Zhao, L. X.; Liang, X.; Lei, Y. M.; Luo, Y. H. Structure and Magnetic Properties of La-Doped Si_n (n = 1−12, 24) Clusters: A Density Functional Theory Investigation. *Eur. Phys. J. D* **2008**, *49*, 343−351.

(41) (a) Sporea, C.; Rabilloud, F. Stability of Alkali-Encapsulating Silicon Cage Clusters. *J. Chem. Phys.* **2007**, *127*, 164306/01−07. (b) Sporea, C.; Rabilloud, F.; Cosson, X.; Allouche, A. R.; Aubert-Frecon, M. Theoretical Study of Mixed Silicon−Lithium Clusters $Si_nLi_p^{(+)}$ (n = 1−6, p = 1−2). *J. Phys. Chem. A* **2006**, *110*, 6032−6038. (c) Sporea, C.; Rabilloud, F.; Allouche, A. R.; Frecon, M. Ab Initio Study of Neutral and Charged $Si_nNa_p^{(+)}$ (n ≤ 6, p ≤ 2) Clusters. *J. Phys. Chem. A* **2006**, *110*, 1046−1051.

(42) Koyasu, K.; Atobe, J.; Akutsu, M.; Mitsui, M.; Nakajima, A. Electronic and Geometric Stabilities of Clusters with Transition Metal Encapsulated by Silicon. *J. Phys. Chem. A* **2007**, *111*, 42−49.

(43) Janssens, E.; Gruene, P.; Meijer, G.; Woste, L.; Lievens, P.; Fielicke, A. Argon Physisorption As Structural Probe for Endohedrally Doped Silicon Clusters. *Phys. Rev. Lett.* **2007**, *99*, 063401.

(44) Dmytruk, A.; Park, Y. S.; Kasuya, A.; Kikuchi, H.; Takahashi, M.; Kawazoe, Y.; Watanabe, A. Silicon Subiodide Clusters. *J. Nanosci. Nanotechnol.* **2007**, *7*, 3788−3791.

(45) (a) Nigam, S.; Majumder, C.; Kulshreshtha, S. K. Structural and Electronic Properties of Si_n, Si_n^+, and $AlSi_{n-1}$ (n = 2−13) Clusters: Theoretical Investigation Based on ab Initio Molecular Orbital Theory. *J. Chem. Phys.* **2004**, *121*, 7756. (b) Majumder, C.; Kulshreshtha, S. K. Influence of Al Substitution on the Atomic and Electronic Structure of Si Clusters by Density Functional Theory and Molecular Dynamics Simulations. *Phys. Rev. B* **2004**, *69*, 115432. (c) Nigam, S.; Majumder, C.; Kulshreshtha, S. K. Structural and Electronic Properties of Si_n, Si_n^-, and PSi_{n-1} Clusters: Theoretical Investigation Based on ab Initio Molecular Orbital Theory. *J. Chem. Phys.* **2006**, *125*, 074303.

(46) Ma, L.; Zhao, J.; Wang, J.; Wang, B.; Lu, Q.; Wang, G. Growth Behavior and Magnetic Properties of Si_nFe (n = 2−14) Clusters. *Phys. Rev. B* **2006**, *73*, 125439.

(47) Ngan, V. T.; Gruene, P.; Claes, P.; Janssens, E.; Fielicke, A.; Nguyen, M. T.; Lievens, P. Disparate Effects of Cu and V on Structures of Exohedral Transition Metal-Doped Silicon Clusters: A Combined Far-Infrared Spectroscopic and Computational Study. *J. Am. Chem. Soc.* **2010**, *132*, 15589−15602.

(48) Tam, N. M.; Ngan, V. T.; de Haeck, J.; Bhattacharyya, S.; Le, H. T.; Janssens, E.; Lievens, P.; Nguyen, M. T. Singly and Doubly Lithium Doped Silicon Clusters: Geometrical and Electronic Structures and Ionization Energies. *J. Chem. Phys.* **2012**, *136*, 024301.

(49) Ngan, V. T.; Nguyen, M. T. The Aromatic 8-Electron Cubic Silicon Clusters $Be@Si_8$, $B@Si_8^+$, and $C@Si_8^{2+}$. *J. Phys. Chem. A* **2010**, *114*, 7609−7615.

(50) Tam, N. M.; Tai, T. B.; Nguyen, M. T. Thermochemical Parameters and Growth Mechanism of the Boron-Doped Silicon Clusters, Si_nB^q with n = 1−10 and q = −1, 0, +1. *J. Phys. Chem. C* **2012**, *116*, 20086−20098.

(51) Ngan, V. T.; Janssens, E.; Claes, P.; Lyon, J. T.; Fielicke, A.; Nguyen, M. T.; Lievens, P. High Magnetic Moments in Manganese-Doped Silicon Clusters. *Chem.—Eur. J.* **2012**, *18*, 15788−15793.

(52) Ngan, V. T.; Pierloot, K.; Nguyen, M. T. $Mn@Si_{14}^+$: A Singlet Fullerene-Like Endohedrally Doped Silicon Cluster. *Phys. Chem. Chem. Phys.* **2013**, *15*, 5493−5498.

(53) Kawamura, H.; Kumar, V.; Kawazoe, Y. Growth Behavior of Metal-Doped Silicon Clusters Si_nM (M = Ti,Zr,Hf; n = 8−16). *Phys. Rev. B* **2005**, *71*, 075423.

(54) Reis, C. L.; Pacheco, J. M. Bulk Materials Made of Silicon Cage Clusters Doped with Ti, Zr, or Hf. *J. Phys.: Condens. Matter* **2010**, *22*, 035501−.

(55) Majumder, C.; Kulshreshtha, S. K. Impurity-Doped Si_{10} Cluster: Understanding the Structural and Electronic Properties from First-Principles Calculations. *Phys. Rev. B* **2004**, *70*, 245426.

(56) Landman, U.; Barnett, R. N.; Scherbakov, A. G.; Avouris, P. Metal-Semiconductor Nanocontacts: Silicon Nanowires. *Phys. Rev. Lett.* **2000**, *85*, 1958−1961.

(57) Kotlyar, V. G.; Zotov, A. V.; Saranin, A. A.; Kasyanova, T. V.; Cherevik, M. A.; Pisarenko, I. V.; Lifshits, V. G. Formation of the Ordered Array of Al Magic Clusters on Si(111)7 × 7. *Phys. Rev. B* **2002**, *66*, 165401.

(58) Paulose, M.; Grimes, C. A.; Varghese, O. K.; Dickey, E. C. Self-Assembled Fabrication of Aluminum−Silicon Nanowire Networks. *Appl. Phys. Lett.* **2002**, *81*, 153−155.

(59) Sun, Z.; Yang, Z.; Gao, Z.; Tang, Z. C. Experimental and Theoretical Investigation on Binary Semiconductor Clusters of B/Si and Al/Si. *Rapid. Commun. Mass. Spectrom.* **2007**, *21*, 792−798.

(60) Li, B.; Wang, G.; Ye, M.; Yang, G.; Yao, C. Geometric and Energetic Properties of Al-Doped Si_n (n = 2−21) Clusters: FP-LMTO-MD Calculations. *J. Mol. Struct.* **2007**, *820*, 128−140.

(61) Frisch, M. J.; Schlegel, H. B.; Scuseria, G. E.; Robb, M. A.; Cheeseman, J. R.; Montgomery, J. A., Jr.; Vreven, T.; Kudin, K. N.; Burant, J. C.; Millam, J. M.; et al. *Gaussian 09*, revision B.01; Gaussian, Inc.: Wallingford, CT, 2009.

(62) Werner, H-J; Knowles, P. J.; Lindh, R.; Manby, F. R.; Schütz, M.; Celani, P.; Korona, T.; Rauhut, G.; Amos. R. D.; et al. *MOLPRO, version 2006.1, a package of ab initio programs*, 2009.

(63) Tai, T. B.; Nguyen, M. T. A Stochastic Search for the Structures of Small Germanium Clusters and Their Anions: Enhanced Stability by Spherical Aromaticity of the Ge_{10} and Ge_{12}^{2-} Systems. *J. Chem. Theor. Comput.* **2011**, *7*, 1119−1130.

(64) Clark, T.; Chandrasekhar, J.; Spitznagel, G. W.; Schleyer, P. V. Efficient Diffuse Function-Augmented Basis Sets for Anion Calculations. III. The 3-21+G Basis Set for First-Row Elements, Li−F. *J. Comput. Chem.* **1983**, *4*, 294−301.

(65) McLean, A. D.; Chandler, G. S. Contracted Gaussian Basis Sets for Molecular Calculations. I. Second Row Atoms, Z = 11−18. *J. Chem. Phys.* **1980**, *72*, 5639−5648.

(66) Frisch, M. J.; Pople, J. A.; Binkley, J. S. Self-Consistent Molecular Orbital Methods 25. Supplementary Functions for Gaussian Basis Sets. *J. Chem. Phys.* **1984**, *80*, 3265−3269.

(67) Peterson, K. A.; Xantheas, S. S.; Dixon, D. A.; Dunning, T. H. Predicting the Proton Affinities of H_2O and NH_3. *J. Phys. Chem. A* **1998**, *102*, 2449−2454.

(68) Curtiss, L. A.; Redfern, P. C.; Raghavachari, K. Gaussian-4 Theory. *J. Chem. Phys.* **2007**, *126*, 084108.

(69) (a) Tai, T. B.; Grant, D. J.; Nguyen, M. T.; Dixon, D. A. Thermochemistry and Electronic Structure of Small Boron Clusters (B_n, n = 5−13) and Their Anions. *J. Phys. Chem. A* **2010**, *114*, 994−1007. (b) Nguyen, M. T.; Matus, M. H.; Ngan, V. T.; Grant, D. J.; Dixon, D. A. Thermochemistry and Electronic Structure of Small Boron and Boron Oxide Clusters and Their Anions. *J. Phys. Chem. A* **2009**, *113*, 4895−4909. (c) Tai, T. B.; Tam, N. M.; Nguyen, M. T. The Boron Conundrum: The Case of Cationic Clusters B_n^+ with n = 2−20. *Theor. Chem. Acc.* **2012**, *131*, 1241 and references therein.

(70) Bartlett, R. J.; Musial, M. Coupled-Cluster Theory in Quantum Chemistry. *Rev. Mod. Phys.* **2007**, *79*, 291−352.

(71) (a) Dunning, T. H. Gaussian Basis Sets for Use in Correlated Molecular Calculations. I. The Atoms Boron through Neon and Hydrogen. *J. Chem. Phys.* **1989**, *90*, 1007−1023. (b) Kendall, R. A.; Dunning, T. H.; Harrison, R. J. Electron Affinities of the First-Row Atoms Revisited. Systematic Basis Sets and Wave Functions. *J. Chem. Phys.* **1992**, *96*, 6796−6806. (c) Woon, D. E.; Dunning, T. H. Gaussian Basis Sets for Use in Correlated Molecular Calculations. III. The Atoms Aluminum through Argon. *J. Chem. Phys.* **1993**, *98*, 1358−1371.

(72) Rittby, M.; Bartlett, R. J. An Open-Shell Spin-Restricted Coupled Cluster Method: Application to Ionization Potentials in Nitrogen. *J. Phys. Chem.* **1988**, *92*, 3033−3036.

(73) Deegan, M. J. O.; Knowles, P. Perturbative Corrections to Account for Triple Excitations in Closed and Open Shell Coupled Cluster Theories. *Chem. Phys. Lett.* **1994**, *227*, 321−326.

(74) Peterson, K. A.; Dunning, T. H., Jr. Accurate Correlation Consistent Basis Sets for Molecular Core−Valence Correlation Effects: The Second Row Atoms Al−Ar, and the First Row Atoms B−Ne Revisited. *J. Chem. Phys.* **2002**, *117*, 10548−10560.

(75) (a) Helgaker, T.; Klopper, W.; Koch, H.; Noga, J. Basis-Set Convergence of Correlated Calculations on Water. *J. Chem. Phys.* **1997**, *106*, 9639−9646. (b) Halkier, A.; Helgaker, T.; Jorgensen, P.; Klopper, W.; Koch, H.; Olsen, J.; Wilson, A. K. Basis-Set Convergence in Correlated Calculations on Ne, N_2, and H_2O. *Chem. Phys. Lett.* **1998**, *286*, 243−252.

(76) (a) Douglas, M.; Kroll, N. M. Quantum Electrodynamical Corrections to the Fine Structure of Helium. *Ann. Phys.* **1974**, *82*, 89−155. (b) Hess, B. A. Applicability of the No-Pair Equation with Free-Particle Projection Operators to Atomic and Molecular Structure Calculations. *Phys. Rev. A* **1985**, *32*, 756−763. (c) Hess, B. A. Relativistic Electronic-Structure Calculations Employing a Two-Component No-Pair Formalism with External-Field Projection Operators. *Phys. Rev. A* **1986**, *33*, 3742−3748.

(77) de Jong, W. A.; Harrison, R. J.; Dixon, D. A. Parallel Douglas−Kroll Energy and Gradients in NWChem: Estimating Scalar Relativistic Effects Using Douglas−Kroll Contracted Basis Sets. *J. Chem. Phys.* **2001**, *114*, 48−53.

(78) EMSL basis set library. http://www.emsl.pnl.gov/forms/basisform.html.

(79) Moore, C. E. *Atomic Energy Levels As Derived from the Analysis of Optical Spectra, Vol. 1, H to V*; U.S. National Bureau of Standards Circular 467; U.S. Department of Commerce, National Technical Information Service, COM-72-50282: Washington, D.C., 1949.

(80) Karton, A.; Martin, J. M. L. Heats of Formation of Beryllium, Boron, Aluminum, and Silicon Re-Examined by Means of W4 Theory. *J. Phys. Chem. A* **2007**, *111*, 5936−5944.

(81) Curtiss, L. A.; Raghavachari, K.; Redfern, P. C.; Pople, J. A. Assessment of Gaussian-2 and Density Functional Theories for the Computation of Enthalpies of Formation. *J. Chem. Phys.* **1997**, *106*, 1063−1079.

(82) Knight, L. B.; McKinley, A. J.; Babb, R. M.; Morse, M. D.; Arrington, C. A. Laser Vaporization Generation of the SiB and SiAl Radicals for Matrix Isolation Electron Spin Resonance Studies; Comparison with Theoretical Calculations and Assignment of Their Electronic Ground States as $X^4\Sigma$. *J. Chem. Phys.* **1993**, *98*, 6749−6757.

(83) (a) Lyon, J. T.; Gruene, P.; Fielicke, A.; Meijer, G.; Janssens, E.; Claes, P.; Lievens, P. Structures of Silicon Cluster Cations in the Gas Phase. *J. Am. Chem. Soc.* **2009**, *131*, 1115. (b) Fielicke, A.; Lyon, J. T.; Haertelt, M.; Meijer, G.; Claes, P.; De Haeck, J.; Lievens, P. Vibrational Spectroscopy of Neutral Silicon Clusters via Far-IR-VUV Two Color Ionization. *J. Chem. Phys.* **2009**, *131*, 171105−.

(84) Karamanis, P.; Marchal, R.; Carbonniére, P.; Pouchan, C. Doping Effects on the Electric Response Properties of Silicon Clusters: A Global Structure−Property Investigation of $AlSi_{n-1}$ Clusters (n = 3−10). *Chem. Phys. Lett.* **2010**, *500*, 59−64.

(85) Yang, J. C.; Xu, W. G.; Xiao, W. S. The Small Silicon Clusters Si_n (n = 2−10) and Their Anions: Structures, Themochemistry, and Electron Affinities. *J. Mol. Struct.* **2005**, *719*, 89−102.

(86) Zdetsis, A. D. Analogy of Silicon Clusters with Deltahedralboranes: How Far Can It Go? Reexamining the Structure of Si_n and Si_n^{2-}, n = 5−13 Clusters. *J. Chem. Phys.* **2007**, *127*, 244308/01−06.

(87) Brack, M. The Physics of Simple Metal Clusters: Self-Consistent Jellium Model and Semiclassical Approaches. *Rev. Mod. Phys.* **1993**, *65*, 677−732.